Master's thesis

Master's thesis 2019 Eirik Nedkvitne

NTNU
Norwegian University of
Science and Technology
Faculty of Natural Sciences
Department of Materials Science and Engineering

Eirik Nedkvitne

Leaching and Precipitation Experiments Related to the Pedersen Process

June 2019

NTNU
Norwegian University of
Science and Technology

NTNU
Norwegian University of
Science and Technology

NTNU
Norwegian University of
Science and Technology

Leaching and Precipitation Experiments Related to the Pedersen Process

Eirik Nedkvitne

Materials Science and Engineering
Submission date: June 2019
Supervisor: Leiv Kolbeinsen
Co-supervisor: Jafar Safarian

Norwegian University of Science and Technology
Department of Materials Science and Engineering

Abstract

Large amount of residual red mud is generated from the production of metallurgical grade alumina from the commercial Bayer process. Environmental challenges are associated with landfilling the residue. An alternative route for alumina production is via the Pedersen process. It is a combined pyro- and hydrometallurgical process for producing alumina which avoids the generation of residues. The total environmental impact is lower for an optimized Pedersen process compare to the present Bayer process. This Thesis explore the system of carbonization of sodium aluminate solutions and leaching characteristics of calcium aluminate slags related to the Pedersen process. Experiences related to carbonization experiments are shared and key features for carbonization of sodium aluminate solutions are presented. This Thesis forms a basis for further research that may lead to more sustainable alumina production.

Sammendrag

Store mengder avfall rødslam generes fra produksjon av metallurgisk aluminiumoksid via den nåværende kommersielle Bayer prosessen. Deponering av avfallet byr på miljøutfordringer. Alternativt kan aluminiumoksid produseres via Pedersen prosessen. Dette er en kombinert hydro- og pyrometallurgisk prosess som fremstiller oksidet uten avfallsprodukter. Det totale miljøfotavtrykket for en moderne Pedersen prosess er lavere enn Bayer prosessen. Denne avhandlingen utforsker systemet knyttet til karbonisering av natriumaluminat løsninger og karakteristikk av grå slam relatert til Pedersen prosessen. Erfaringer relatert til karboniserings eksperimenter og hoved aspekter knyttet til karboniseringsprosessen blir presentert. Denne masteroppgaven danner et grunnlag for videre forsking som kan lede til mer miljøvennlig produksjon av aluminiumoksid.

Preface and acknowledgment

This Thesis concludes my master's degree in Material Science and Engineering at the Department of Material Science and Engineering at the Norwegian University of Technology and Science. This is a worthy end to a 5 years long journey of studying material science and process metallurgy.

I experienced early in the process that doing research takes time. It is a continuous process of making mistakes at the lab, searching for appropriate literature, re-reading perplexing literature found months before and discussing interesting problems with fellow researchers. The more I have learned about the process studied, the more I have discovered how little I know and the more I want to find out. I felt that I have only scratched the surface of an interesting research topic.

It is difficult to avoid hidden traps when exploring new terrain. Many mistakes have been done throughout the work and disappointment was felt when important samples were ruined, or when the experimental set-up did not work as planned. I wanted to write an honest Thesis not holding back mistakes, but rather pass on experiences to the reader.

The work is within the EnsureAl project which has received funding from the European Community's Horizon 2020 Programme. The project information can today be found at https://www.ensureal.com/. I feel privileged as a Master's student to be allowed to join the project meeting in Poland in March this year.

I would like to thank my supervisor Leiv Kolbeinsen for introducing me for an interesting Thesis topic that has motivated me to work hard. I feel very fortunate to explore the science behind hydrometallurgy as this has broadened my competence in process metallurgy. My co-supervisor Jafar Safarian deserves acknowledgement for the continuous good guidance throughout the semester. I have appreciated the regularly meetings where the progress of my work has been discussed. I would also like to give a special thanks to PhD candidate Fabian Azof for good discussions and guidance throughout the work. Without him this work would have been significantly more challenging. Also, the department engineer Ivar Andre Ødegård and Arman Kermani have given me invaluable help at the lab. I would also like to thank the

SiManTi group for being an excellent arena for young researchers. I think sharing experiences and the collaboration brings science foreword. I would also thank Irmeline de Sadeleer for all the support.

I hope you will enjoy your reading and find the topic interesting!

Eirik Nøst Nedkvitne, June 6. 2019.

Table of contents

List of figures

List of tables

List of materials

Alumina	Al_2O_3
Calcium carbonate	$CaCO_3$
Bayerite	$Al(OH)_3$, $Al_2O_3.3H_2O$
Boehmite	AlO(OH), , $Al_2O_3.H_2O$
Gibbsite	$Al(OH)_3$, $Al_2O_3.3H_2O$
Grossite	CA2, $CaO.2Al_2O_3$
Lime	CaO
Katoite	$Ca_3Al_2(OH)_2$
Krotite	CA, $CaO.Al_2O_3$, $CaAl_2O_4$
Mayenite	C12A7, $12CaO.7Al_2O_3$
Monocarboaluminate	CA4ACH13, $Ca_4Al_2(CO_3)(OH)_{12}(H_2O)_5$
Nordstrandite	$Al(OH)_{3,}$, $Al_2O_3.3H_2O$
Silica	SiO_2
Sodium carbonate	Na_2CO_3
Sodium hydroxide	NaOH
Sodium aluminate	$NaAl(OH)_4$
Tri calcium aluminate	C3A, $3CaO.Al_2O_3$

Abbreviations

IAI	The International Aluminums Institute
ICP-MS	Inductively coupled mass spectroscopy
LDA	Laser diffraction analysis
PDF	Powder Diffraction File™
pH	pondus Hydrogenii
SEM	Scanning electron microscope
XRD	X-ray powder diffraction
XRF	X-ray fluorescence

1 Introduction

Aluminium is the second most produced metal in the world. The demand for the light metal has significantly increased the last decades. The International Aluminium Institute (IAI) reported that 64 000 thousand metric tons of primary alumina was produced world-wide in 2018. This is a 2.6-fold increase since 2000. Its strength, light weight and good functional properties makes it suitable and desired for advanced and innovative technologies.

Aluminium is produced by molten salt electrolysis. Large amount of electricity is used to reduce aluminium oxide (alumina) in a cryolite bath with carbon anodes. About 2 kg of alumina is needed to produce 1 kg of aluminium, which again is produced from about 5 kg of bauxite. The bauxite ore is a sedimentary rock that is often found near the surface terrain. Strip mining is therefore the preferred method of mining. Gangue minerals in the bauxite is separated from aluminium hydroxide minerals by alkaline leaching and crystalized aluminium hydroxide is then calcined into alumina in large rotary kiln furnaces.

Each process step has environmental impacts. Land use and ecosystem disturbance is the major impacts from the mining process; chemical pollution and residue deposition the major challenges for alumina production process and air pollution and energy usage the ones from the electrolysis process. Improving the environmental performance from the value chain can make up a significant difference due to the size and importance of the aluminium industry.

Almost all metallurgical alumina today is produced by the well-known Bayer process. The performance of the Bayer process is highly dependent of the characteristics of the bauxite. Ore containing less leachable compounds require higher operation temperatures and increases the process energy usage. Ores with impurities like silica lead to lower alumina yield and higher caustic soda consumption. The Bayer process has therefore limitations when it comes to processing low-grade bauxites but is economical superior when it comes to processing high quality equatorial lateritic bauxites. Another challenge with the Bayer process is generation of process residue called red-mud. Large amounts of residue must be carefully handled. This can be costly and environmentally harmful if not done properly. During the last decade new motivation for looking at alternative processes to the Bayer process has arisen. This as a result of an increasing red-mud challenge with a larger focus on developing processes within a circular economy, reduce total environmental impacts throughout value chains and ensuring supply risk for a rapidly increasing demand.

The Pedersen process is an alternative method for producing alumina. This process utilizes ferruginous bauxites to produce both alumina and cast iron. Iron compounds in bauxite are carbothermal reduced to metallic iron and alumina is extracted from a high alumina rich slag with a leaching process. There is no residue related to the process as the material left from leaching (grey mud) can be used in farming or construction industry. Combined processes utilising hydrometallurgical and pyrometallurgical methods makes it possible to exploit process synergies with lower energy consumption and reduce CO_2 emission. The environmental performance of a modern Pedersen process is superior to the Bayer process when impacts related to by-products are taken into account. A larger variety of bauxite qualities can also be processed by the Pedersen process. This can for example give the flexibility to choose sustainable mining location or use deposits that are closer located to the aluminium plants, reducing transport costs and impacts. The flexibility of the process can also be favourable for ensuring supply risk for certain areas with alumina smelters.

The Pedersen process was already developed in 1927. There is little novel literature on old processes like the Pedersen process. Some of the old literature is not digitalized and can therefore be hard to find. Some of the experimental work described in old literature could be reproduced with new measuring techniques and characterisation methods to describe the system better. New scientific work could put new light on the process or lead to new innovative process solutions beneficial for the today worldview. The aim of this Thesis is to contribute to increased knowledge on the Pedersen process that may lead to a more sustainable alumina production. The economical sustainability of the process is an important factor for a possible process start up. Therefore, aspects related to a highly productive version of the Pedersen process are studied.

Most of the resent scientific effort for precipitate aluminium hydroxide from sodium aluminate solutions are related to optimizing the commercial Bayer process. The method used does not use carbonization of the solution to provoke precipitation. Novel documentation is therefore needed for the method based on carbonation with CO_2 purging used in the Pedersen process. This Thesis aims at exploring the system for precipitation of aluminium hydroxide with carbonisation according to the Pedersen process. It wants to give further research a solid foundation for executing relevant experiments by building a simple experimental set-up and highlight key process features. The Thesis tries to give a holistic view of the process, taking into account aspects beneficial for slag making, leaching and precipitation. Both leaching and

precipitation experiments are performed. The leaching behaviour for different kinds of slag are therefore also a crucial part of the Thesis. Slag making has been documented by the author's previous work (Nedkvitne, 2018) or obtained from work running simultaneously from the EnsureAl project. Some part of this report shares same paragraphs as the authors preliminary work.

Chapter 2 presents alumina production processes. This is essential for assessing if the Pedersen process can be competitive or sustainable. First, the chapter gives a short summary of alternative alumina processes. Second, new ideas and concepts from similar processes that can give rise to innovative solutions creating smart variations of existing processes are presented. Chapter 3 introduces the theory needed for understanding what happens during the experiments. Chapter 4 presents the experimental method and how this developed throughout this work. Experimental results are presented in Chapter 5 with following discussion of alumina extraction, grey mud characteristics, precipitation yield, precipitate characteristics, particle size distribution and silica contamination in Chapter 6.

2 Background information

2.1 Bauxite

Bauxite is the principal ore for aluminium production. The ore is formed during intense weathering and erosion of a parent rock near the earth surface. Certain climatic conditions over a prolonged time result in bauxite formation. Bauxite consist of hydrated alumina minerals with variable proportions of iron oxides, silica and titan oxides. The alumina hydrates formed can be gibbsite, boehmite or diaspore. Gibbsite is easier to digest in caustic soda than boehmite and diaspore. The mineral composition of the bauxite is therefore crucial for the performance of the Bayer process. Bauxites are classified into lateritic and karst types. In general, karst bauxites constitute more likely of boehmite and minerals that are difficult to process. As a result, almost 90% of the exploited reserves today consist of lateritic bauxites (Smith, 2009). Meyer (2004) gives a good overview of global bauxite reserves estimated in 2004. Figure 1 shows karst and laterite bauxite reserve distribution in the world. The estimated tonnage suitable for the Bayer process is estimated from the CRC 525 database. Large proportions of the karst bauxites are located in Europe.

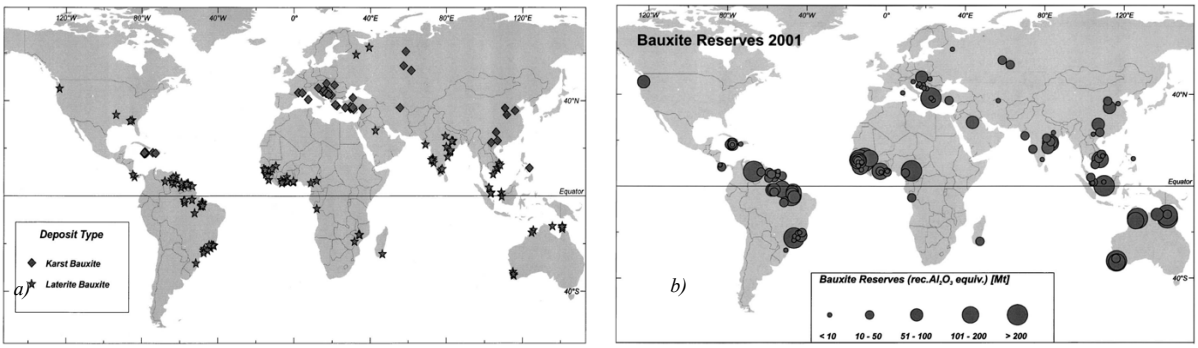

Figure 1. Map of bauxite reserves. *a*) Located karst bauxites and laterite bauxite reserves. b) Tonnage of recoverable alumina with the Bayer process. Ref. (Meyer, 2004)

Iron compounds are an unwanted species for the Bayer process but is essential for the Pedersen as pig iron is separated as a valuable by product. A substantial amount of iron can be found in lateritic ores. The chemical composition of 69 lateritic bauxites was analysed by Aleva (1994) and the iron oxide content varied from 3.9 - 69.8% with a mean content of 21.2%. Bauxite with a high iron oxide content is called ferruginous bauxites.

The location of bauxite reserves can play an important role for the aluminium value chain. Aluminium electrolysis plants are often located where it is a reliable access to cheap electricity.

This is not always near bauxite reserves. Mines closer to aluminium plants with cheaper electricity reduce transportation costs.

Ensuring supply lines is essential for ore processing industries. Importing ores from mines located near political unstable mining areas or from areas where competitions is too high due to geopolitical conflicts are associated with high risk. Higher demands for environmentally friendly mining around the world can also lead to supply line problems. Strip mining processes can often be controversial because in many cases large areas must be used for extracting thin layers of ore. The competitions from mines that are the most sustainable mining can increase. Malaysia banned bauxite mining from 2016 to 2019 as a result of environmental impacts. Run-offs from unsecured stockpiles contaminated water sources and unregulated mining became a large problem for communities around the rapid increasing industry.

2.2 Alumina production

2.2.1 The Bayer process

The Bayer process was invented in 1888 by Carl Josef Bayer. It's a good optimized process as it has been the principal process for alumina production for decades. Figure 2 is a simplified flowsheet of the process. The bauxite is leached with a NaOH solution in pressure vessels. The operation temperature is dependent on the quality of the bauxite; around 220-270°C for bauxite constituting of boehmite and diaspore and around 150°C for bauxite primarily constituting of gibbsite (Power, Gräfe and Klauber, 2011). Undissolved minerals and compounds are filtered out to form the process residue called red-mud. Precipitation of aluminium hydroxide is performed by lowering temperature and pressure to supersaturate the leachate. Seeds are added to facilitate auto precipitation.

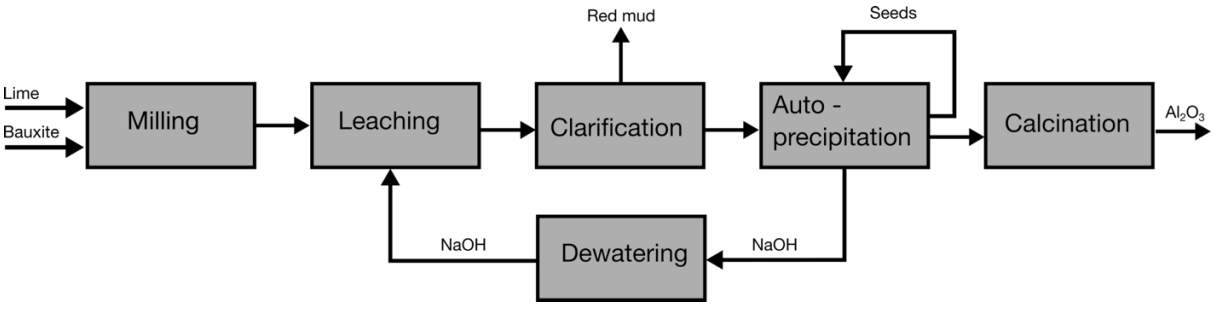

Figure 2. Simplified flowsheet of the Bayer process.

Silica is the main impurity in the Bayer process because of the high solubility of the compound in alkaline solutions. Therefore, in many processes today a pre-desilication stage is performed before leaching (Smith, 2009). A slurry of bauxite and spent liquor are stored at near

atmospheric boiling point to encourage reprecipitation of dissolved silica to desilication products. These products, also constituting of sodium and alumina, are discarded with the red-mud. This is resulting in a lower alumina yield, increased sodium loss and a more toxic red-mud. Usually a bauxite with higher reactive silica content than 8% is considered to be uneconomic.

2.2.2 Red mud

Disposal of red-mud is one of the major environmental challenges within the aluminium value chain. Issues related to red-mud are well covered by a series of reviews (Gräfe and Klauber, 2011; Gräfe, Power and Klauber, 2011; Klauber, Gräfe and Power, 2011; Power, Gräfe and Klauber, 2011). Red mud has no economic value and are disposed in lagoons, in dry stacks or in marine deposits. Due to its low viscosity and high alkalinity, leakage from storages to surrounding ecosystems or ground water can lead to serious environmental damages. Average untreated bauxite residue has a pH of 11.2 ± 1 and seepage from dry stacks to ground water can for example appear after heavy rainfalls. Significant expenses are needed to carefully handle the red-mud. Acid neutralisation is a common way of making red mud harmless, but this can increase expenses significantly. Researchers have looked at the potential to reprocess the red mud into valuable products. For example as Zhang *et al.* (2018) investigated recovery of iron and alumina from the residue. The lack of careful storage has led to several accidents the previous decade. Ajika alumina plant in October 2010 and Wanji alumina plant august 2016 experienced dam breakages that led to severe consequences. The Alunorte bauxite refinery in Brazil had to be run on half capacity in 2019 as a result of accusations of water pollution and not sufficient careful handling of red-mud landfill during heavy raining.

2.2.3 Alternative methods

Finding alternative methods for producing alumina is more relevant now as access to quality bauxite globally decreases with an increased global aluminium demand. Also, because alternative methods can possibly operate in a more environmentally friendly way than the existing Bayer process. Senyuta, et al. (2013) points out the need for new innovative technologies to process low grade bauxites or alumina rich non-bauxitic rocks like kaolinite. They emphasise the increased global competition for high quality bauxites and long transport distances from bauxite refineries to aluminium smelters. Their paper goes through how alkaline methods to process low grade ores into alumina has developed and present alternative acidic

methods. A process using hydrochloric acid is stated to be the most economical feasible for the acidic processes.

Peter Smith (2009) review the existing and potential alkaline based processes for high silica bauxites. Possible solutions for how the Bayer process can be modified to cope with high silica content are also discussed. These modification aims for minimalizing reactive silica input by bauxite pre-treatments, modify the process or recovering soda from the desilication products. Ma and Li (2012) propose a process to recover alumina and soda from the desilication products by and additional leaching step of the first leaching filtrate.

Traditionally alumina has been produced differently in Russia and China. Processes similar to or modification of the Pedersen process have been used. They are based on sintering alumina containing ores with lime to create a sinter with similar chemical structure as the slag obtained in the Pedersen process. This makes it possible to leach the sinter in the same way as the slag used in the Pederson process. Silicon contamination is often problematic, and the processes have often an integrated desilication step. Another challenge with these methods is the high energy use. Typical high-grade bauxite refineries using the Bayer process can produce alumina at 11-13GJ/Al_2O_3, but the sinter process can expect energy cost up to 38 GJ/ Al_2O_3 (Peter Smith, 2009). In the past decades researchers have been focused on adapting the sintering processes for coal fly ash with a high alumina content (Yao *et al.*, 2014). Russia has over 70 years of experience processing nepheline syenite to produce alumina, soda ash, potash and cement (Panov, Vinogradov and Engalychev, 2017), without generating any residues. Processing 4-4.5 ton of nepheline with limestone gives 1 ton of alumina, 0.8 tons of soda ash, 0.3 tons of potash and 10 tons of cement. All products are of good quality and there is no need for using external alkalis in the process since sodium is bound in nepheline syenite. This process can be of interest to the Norwegian reader as Norway has access to large nepheline syenite deposits, cheap energy and has a substantial aluminium smelting industry.

Another interesting process is the novel calcification-carbonation method. This is developed to process low grade diasporic bauxite or red mud from the Bayer process (Zhang *et al.*, 2016). The bauxite is mixed with lime and an alkali liquor in pressure vessels. Alumina is dissolved to an aluminate solution and the bauxite is transformed into different forms of hydro garnets. A carbonation treatment is performed on hydro garnet producing calcium carbonate, calcium silicates and aluminium hydroxides. The aluminium hydroxides can be again selectively

dissolved into an alkali solution. The two aluminate solutions can be decomposed into aluminium hydroxide by for example carbonation.

2.3 The Pedersen process

The Pedersen process has potentially the right feature for sustainable alumina production utilizing ferruginous karst bauxite. Harald Pedersen (1927) patented the process in 1927. The process was run in Høyanger in Norway for around 40 years but was shut down in 1969 due to economic reasons. Miller and Irgens (1974) and Nielsen (1978) describe the plant operation. They claim that the process could be economic competitive if new up-to date process technologies were implemented. Høyanger plant had two small 4MW 3-phase smelting furnaces. The furnaces were open, and all the gas were lost. There was no pretreatment of the calcium or the bauxite to reduce energy consumption. In other the words the plant was inefficient when comparing them to today's standards. The papers claim that utilizing modern smelting technology the electricity consumption per output material can be increased by a factor of 2.5 compare to Høyanger operations.

The Pedersen process is a combined pyro- and hydrometallurgical process where the whole ore is exploited. A simplified flow sheet of the process is shown in Figure 3.

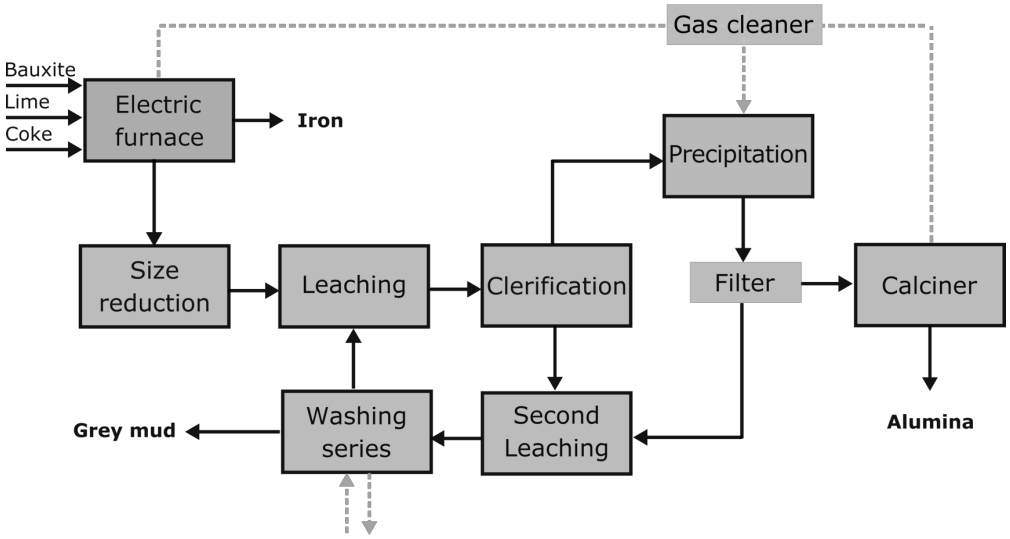

Figure 3. Flowsheet of the Pedersen process.

First, bauxite, lime (CaO) and coke (C) are melted in an electric arc furnace. The iron oxides in the bauxite are reduced into metallic iron and a calcium aluminate slag is formed. The lime is added to obtain a slag suitable for leaching. The pulverized slag is separated from the iron and solidified. The size reduction of the slag occurs in terms of a self-disintegration process upon aging or by mechanical crushing. The slag is then leached in a sodium carbonate solution at 50-100°C under atmospheric pressure. Aluminium dissolves into the solution leaving a residue consisting primarily of calcium carbonates. The calcium carbonate is formed when sodium carbonate reacts with calcium aluminates in the slag. The sodium aluminate solution is separated from the residue and threated in a carbonization process. Carbon dioxide gas is purged through the solution, absorbed to carbonate ions and the sodium aluminate solution decomposed into aluminium hydroxide by crystallisation. The precipitate is calcined and transformed into metallurgical grade alumina. The solution left after precipitation is used in a second leaching step treating the residue from the first leaching step. Unreacted slag from the first leaching step reacts with the solution low concentration of sodium aluminate and high concentration of sodium carbonate that is reintroduced by the carbonization. The residue is washed in series resulting in grey mud and a solution that that can be used in the first leaching step treating fresh calcium aluminate slag.

Grey mud has the potential of being of economic value as it has the right composition for products used in the farming industry or feedstock to cement clinker. The basicity of the grey mud makes it suitable for soil improving agent where the earth is acidic, and the grey mud can might be used for building elements of the Ytong. It can also be reused as flux in the bauxite smelting step to adjust the composition of the slag. $CaCO_3$ is decomposed to CaO when exposed to elevated temperatures. Gas with a high CO_2 content from the calcination step or from the smelting furnace off gas can be reused for carbonation.

The Pedersen process is more energy intensive than the Bayer process because it adds the smelting step before leaching but can compete with other advantages. The most important advantages are as follow:

1. Valuable by-products are produced with full exploitation of the raw material. No environmental or economical cost are related to red-mud disposal. Processes with no residues is beneficial to a circular economy.

2. Structural composition of bauxites has no effect on alumina extraction efficiency. The composition of the slag can be optimized for leaching and it is therefore possible to use low-grade bauxites. The large flexibility of what kind of ores that can be used gives possibilities to choose ores that have lower environmental impacts related to mining or ores that are located closer to alumina and aluminium plants. This can lead to lower environmental impacts of the value chain or it can lead to lower transportation costs.

3. Potential for optimizing the process with synergies. Waste heat from the electric furnace and calcination furnace can be recovered as heating source for the leachate. CO_2 from furnace off-gas can be used in the precipitation step. Grey mud can be used as flux to change slag composition.

4. Avoid using pressure vessels that often makes leaching more difficult to operate. The operation temperature is under 100°C under normal atmospheric pressure. Process equipment are easier to maintain.

Access to cheap energy will be crucial for a competitive alumina process using the Pedersen process. Another (potential) challenge can be the high lime consumption. The Pedersen process is also somewhat complex. The quality of several products must be taken into account and chemical composition of solutions and material can be challenging. Optimizing a process takes time and comprehensive research is necessary. Especially when it competes with the well optimized Bayer process. The main challenge for commercializing the Pedersen process is to find investors willing to start a plant and optimize the process to produce quality products to a competitive price.

3 Theory

The first part of the chapter concerns literature based on the Pedersen process, with theory on leaching and precipitation. Some thermodynamic calculations performed with HSC software related to the carbonization system are presented. Further, a section about theory related to silica impurities is presented before ending with a section regarding measurement and characterisation techniques.

Chemical formulas are presented with cement notation, which means that oxides are denoted with a letter and e.g. CaO is noted with C and Al_2O_3 with A. Tri calcium aluminate is written as C3A and not as $3CaO.Al_2O_3$ or $Ca_3Al_2O_6$.

3.1 Literature related to the Pedersen process

There is limited amount of literature based directly on the Pedersen process after Harald Pedersen took out the process patent about 90 years ago. Some pilot plants have been described. T.P. Hignett (1947) describes a pilot plant operated in 1947 utilizing a modified Pedersen process from clay containing high amounts of silica. The pilot plant had a high alumina extraction efficiency but had problems controlling constant silica impurity concentration in the final product. Henry Blake et al. (1966) published work for looking at the feasibility of utilising the Pedersen process for ferruginous bauxites of the pacific northwest in USA. Comprehensive leaching experiments were performed on various types of slags with different silica content. Murer Hollum, Addison James and Alexander Semple (1951) claim in their patent that low silica concentration can be achieved with a variation of the Pedersen process using high leaching temperatures and high alkaline concentrations. Grzymek's (1979) patent concerns processing blast furnace slag to create calcium aluminate slags similar to the sintering process and Pedersen process. Nielsen (1978) describes practical aspects for an improved Pedersen process based on experience with the Høyanger plant. The carbothermic reduction of bauxites, the structural of slag and iron products has recently been studied by Safarian and Kolbeinsen, (2016) and Azof, Kolbeinsen and Safarian (2018)

3.2 Leaching of calcium aluminates

3.2.1 Slag composition

The slag composition is crucial for good leaching performance. Figure 4. a) shows the leachability of phases in the Al_2O_3-CaO-SiO_2 phase diagram that are in the scope of the Pedersen process. Slags low in silica with about equal amounts of lime and alumina gives good leachable slags. Figure 4. b) shows the desired slag composition to attain high alumina yield. Intermediate SiO_2 content determined by the bauxite grade or by not sufficient flux addition can lead to the non-soluble phase C2AS (2CaO.Al_2O_3.SiO).

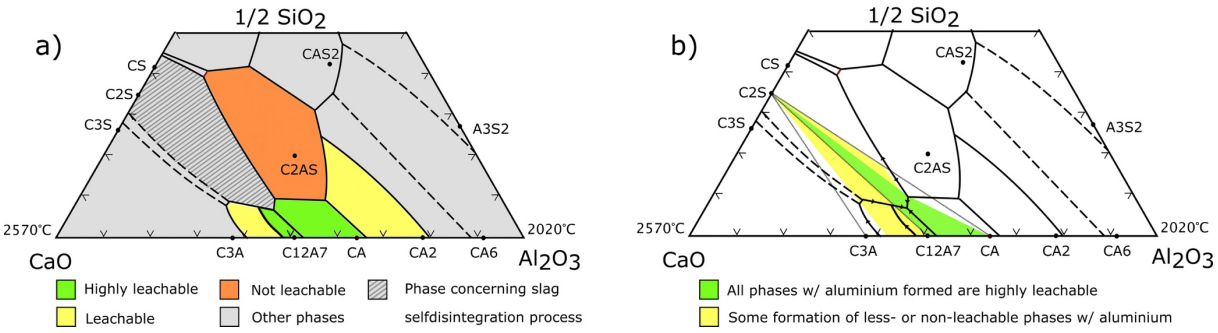

Figure 4. Leachability of phases in the CaO-Al_2O_3-SiO_2 phase diagram. a) Leachability of calcium aluminates in sodium carbonate solution. b) Slag compositions where aluminium atoms are located in highly leachable phases after solidification.

Blake et al.'s (1966) comprehensive study of the leachability of slag obtained by reducing ferruginous bauxite validates the different phase leachabilities in Figure 4. The study also states that bauxites with high titan content have little effect on the leachability. Fabian Azof et al. (2017) investigated the leachability of phases in the mid-range of the Al_2O_3-CaO system and concluded that the leachability of CA (CaO.Al_2O_3, Krotite) is better than C3A (3CaO.Al_2O_3, tricalcium aluminate) that again is better than CA2 (CaO.2Al_2O_3, Grossite). Azof *et al.* (2019) discussing the structure of the calcium aluminate phases and how this may affect the leachabilities.

3.2.2 Leaching conditions

Good leachable phases are characterised by high extraction rates and good selectivity for aluminium compounds. A leaching reaction for a typical slag phase (Krotite, CA, CaO.Al_2O_3) is presented in Equation (1).

$$CaO.Al_2O_3(s) + Na_2CO_3(aq) + 4H_2O\ (l) = 2NaAl(OH)_4(aq) + CaCO_3(s) \qquad (1)$$

Carbonate ions reacts with calcium in the slag phase to form solid $CaCO_3$ during leaching. This frees aluminium ions into solution. Due to the high alkalinity from sodium concentration, all aluminium is present as $NaAl(OH)_4(aq)$. Various leaching conditions have been used in literature (Blake et al., 1966; Miller and Irgens, 1974; Azof, Kolbeinsen and Safarian, 2017). Tong and Li (2008) study optimal leaching conditions for a slag consisting primarily of Mayenite (C12A7, $12CaO.7Al_2O_3$) and states that optimal temperature is equal to 75°C, concentration of Na_2CO_3 equal to 100g/L, holding time equal to 1 hour and liquid to solid ratio equal to 4.5:1. The slag used was made from a pure oxide mixture with same composition as slag originating from red mud smelting. They conclude that the leaching reactions to be inner-diffusion controlled by fitting experimental results to the Avrami equation. The reaction product ($CaCO_3$) deposits on the slag surface and hinder further reactions. They propose a wet milling leaching process for breaking up the $CaCO_3$ layer for enhanced alumina extraction. Improved stirring and agitation could also hinder calcium carbonate deposition. The leaching rate is also highly dependent on slag particle size. A low particle size gives a large total slag-leachate interface i.e. a larger reaction area. Ultrasonic treatment during leaching has some effect for leaching at sub-optimal leaching conditions (Hui-lan et al., 2011). The ultrasound can break up agglomerates and increase the total reaction area. Some leaching conditions found in literature is listed in in Table 1.

Table 1. Leaching condition found in literature.

Reference	Lab/plant	Process	Alakli conc.	Temperature	S:L ratio	Leaching time
H. Pedersen (1927)	Lab	Pedersen process	30-80 g/L	80°C	—	—
Henry E. Blake et al. (1966)	Lab	Pedersen process	44 g/L and 24.5 g/L	25, 45, 65, 90°C	1:16.67 and	Several
K. Nielsen (1978), J. Miller and A. Irgens (1974)	Høyanger plant	Pedersen process, two step leaching	15 g/L	40°C	1:40	5.5h
A. Hollum et. Al (1951)	Lab	Pedersen process, two step leaching	70 -170 g/L	> 80°C	1:3,33	1.5h
Z. Tong and Y. Li (2008)	Lab	Imitation of red mud smelting	100 g/L	75°C	1:4.5	1h 40 min

3.2.3 Grey mud formation and alumina extraction yield

The Pedersen process is a two-step leaching process. First the raw slag is leached with recycled liquor, then the grey mud/unreacted slag is leached with the solution left after carbonatization and precipitation. The second leaching step is important for the yield of the process as the unreacted calcium aluminates will enter the grey mud. The process at the Høyanger plant had a good alumina yield of around 93-95% (and a good iron yield of 95-97%). No literature has been found for leaching slags a second time.

The grey mud composition from the first leaching step can vary with leaching temperature, solid to liquid ratio, alkali concentration etc. Understanding mechanism of grey mud formed is crucial because the formation of calcium carbonate in grey mud determine the alumina extraction rate up to supersaturation limits. A high solid to liquid ration for the first leaching step results in more unreacted slag. However, no unreacted slag was reported from Tong and Li (2008) experiments that used high solid to liquid ratios and had extraction rates between 70 and 84 %. XRD analysis of the residue reported consisted of calcium carbonate and calcium silicate and no aluminium bearing phases. XRD analysis of residue from leaching calcium aluminates (Azof *et al.*, 2019) show unreacted calcium aluminates, calcium carbonates, aluminium hydroxides and hydrated calcium aluminates.

3.3 Precipitation by carbonation

Aluminium hydroxide precipitation by carbonation is an old method and was already used by Le Chatelier as early as in 1855 (Habashi, 2005). Today the method is used for the sinter process and nepheline ore processing. Most of the literature is associated with these two processes, but it is also possible to find some information from the Gryzmec and the Pedersen process.

The solubility of aluminium hydroxides in aqueous solution is highly dependent on pH. At low pH, Al^{3+} is stable and at higher pH, $Al(OH)_4^-$ is stable. In neutral solutions, solid aluminium trihydrate, $Al(OH)_3$, is stable. Equation (2) describes the aluminium hydroxide equilibrium with alkaline solutions.

$$Al(OH)_3(s) + OH^-(aq) = Al(OH)_4^-(aq) \quad (2)$$

The solubility of aluminium hydroxide as function pH can be calculated from the equilibrium constant of Equation (2). The upper plot in Figure 5. shows the maximum concentration of $Al(OH)_4$- ions as function of pH. The equilibrium constants is taken from (J.A. Apps, 1990). The lower plot in Figure 5 shows the Gibbs free energy for Equation (2) as function of temperature illustrating the that the solubility of aluminium hydroxide increases with temperature (calculated with HSC software). Precipitation can occur when the aluminium hydroxide dissolved in the solution is more than that can be dissolved under normal conditions, i.e. when the solution is supersaturated.

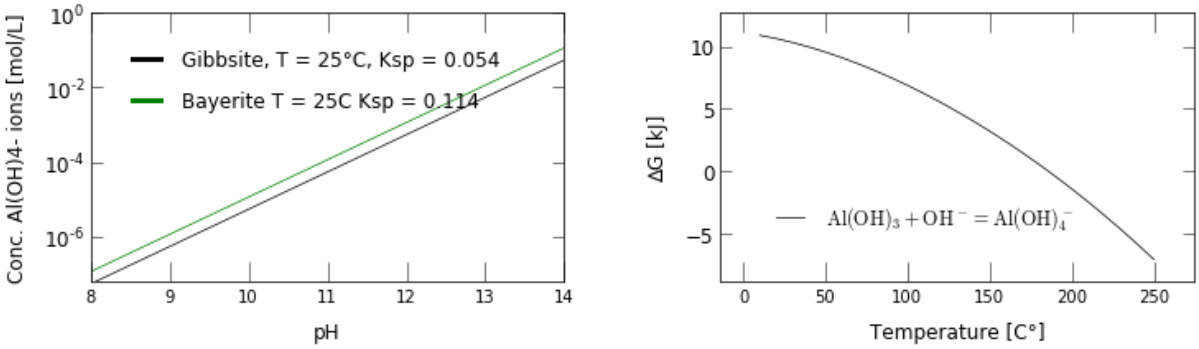

Figure 5. Solubility and driving force for aluminium hydroxide precipitation.

The degree supersaturation can be increased by changing the composition of the solution, e.g. carbonation, or by lowering the temperature or pressure. Figure 6 shows calculated solubility of aluminium as function of pH in comparison with the solubility changing with temperature calculated with fixed pH. The solubility changes faster with pH than temperature change.

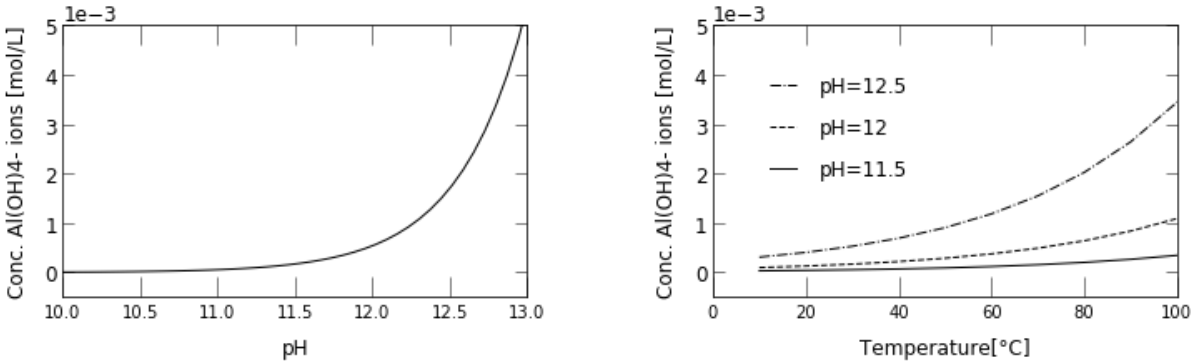

Figure 6. Left plot: $Al(OH)_4^-$ concentration as function of pH. Right plot: $Al(OH)_4^-$ concentration as function of temperature. The pH is very temperature dependent and calculations with fixed pH are not representative.

In the Bayer process aluminium hydroxide precipitation is provoked only by lowering temperature and pressure. In the Pedersen process aluminium hydroxide precipitation is provoked by lowering temperature and lowering pH by carbonation. CO_2 gas is purged through

the solution and absorbed. Carbonate ions are formed and neutralise free NaOH. This leads to hydrolysis of aluminate ions and crystallisation of aluminium hydroxide. The overall reaction of carbonation in alkaline solutions is shown in Equation (3). The overall precipitation reaction can be written as Equation (4). Sodium coupled with aluminium hydroxides transfers to carbonate ions.

$$CO_2(g) + 2OH^-(aq) = CO_3^{-2}(aq) + H_2O(l) \quad (3)$$

$$2NaAl(OH)_4(aq) + CO_2 = Al(OH)_3 + Na_2CO_3(aq) + H_2O \quad (4)$$

Czajkowski, Noworyta and Krotki, (1981) studied aluminium hydroxide precipitation at different carbon dioxide absorption rates. Figure 7 shows how the concentration of reactive species changes throughout carbonation. There are three different regimes during carbonation. In the first stage free sodium hydroxide is neutralised without decomposition of the aluminate ions. In the second stage start the hydrolysis of aluminate ions. In this region aluminium hydroxide precipitates. When the hydroxide concentration is close to zero and bicarbonate ions starts to form, carbonation enters stage 3 and alumina carbonates precipitates (Dawsonite, $NaAlCO_3(OH)_2$). Carbonation used for metallurgical alumina production stops before entering stage 3.

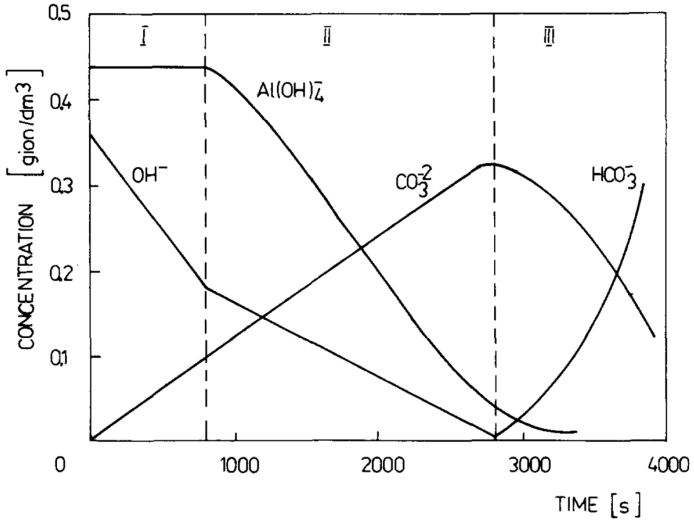

Figure 7. Distribution of reagent concentration in the process of carbonation *(Czajkowski, Noworyta and Krotki, 1981)*.

The concentration ratio of hydroxide ion to aluminate ion effects what phase precipitates from sodium aluminate solutions. Figure 8 (a) shows phase equilibrium lines for different aluminium

hydroxides as function of hydroxide and aluminate ion concentration. It also shows experimental results at different carbonation rates performed by Czajkowski, Noworyta and Krotki, (1981). Figure 8 (b) show the effect of carbonization on hydroxide / aluminate hydroxide ion ratio.

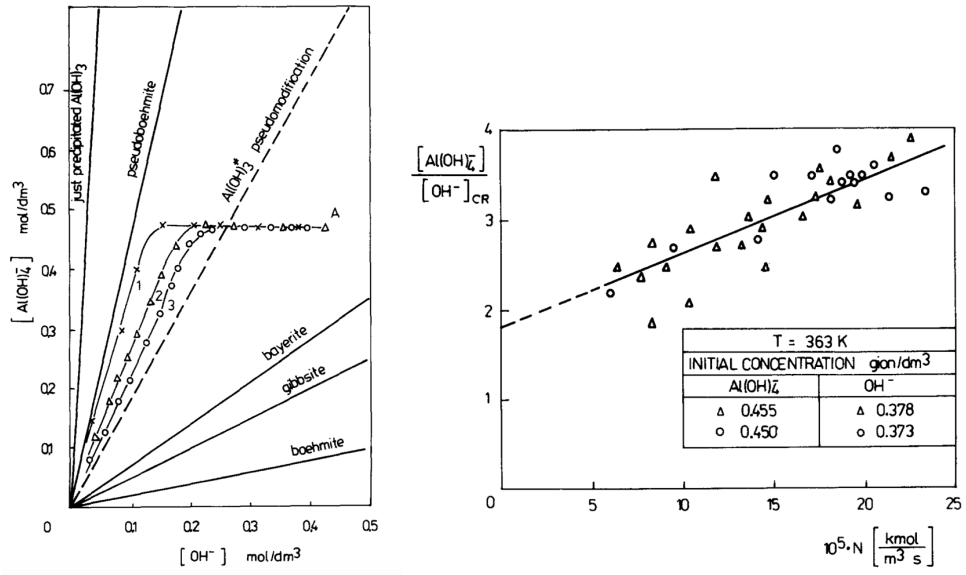

Figure 8. Left plot: Phase equillibrium in aluminate solution – $Al(OH)_3$ as function of ion fraction. Right plot: Ion fraction as function of CO_2 gas flow. Higher gas flow leads to higher $[Al(OH)^{4-}]/[OH^-]$ fraction. (Czajkowski, Noworyta and Krotki, 1981)

Equilibrium calculations executed with the aqua model in HSC is shown in Figure 9. The aqua model utilises the Pitzer method for calculating activity coefficients of ions in aqueous systems. Two different solutions with a low and high alkali concentration with gradually addition of CO_2 are modelled. The calculations show that aluminate ions formed after leaching are not thermodynamically stable and all ions will hydrolyse into aluminium hydroxide. At certain addition of CO_2 when the hydroxide ion concentration reaches low levels dawsonite, $NaAlCO_3(OH)_2$, forms and coexists with aluminium hydroxide. The ratio of dawsonite versus aluminium hydroxide will increase with higher concentration of sodium carbonate, but the appearance of dawsonite will appear at same amounts of absorbed CO_2 for low and high alkali concentration. The plot shows AlO(OH) as the aluminium hydroxide phase. Modelling with $Al(OH)_3$ will give the same results.

The system temperature has little effect on the equilibrium between aluminium hydroxide and dawsonite. Higher temperatures will favourable aluminium hydroxide but not significantly. It's

is worth mentioning that equilibrium calculations might be inaccurate because of the absence of thermodynamically data in aqueous solutions in the HSC database.

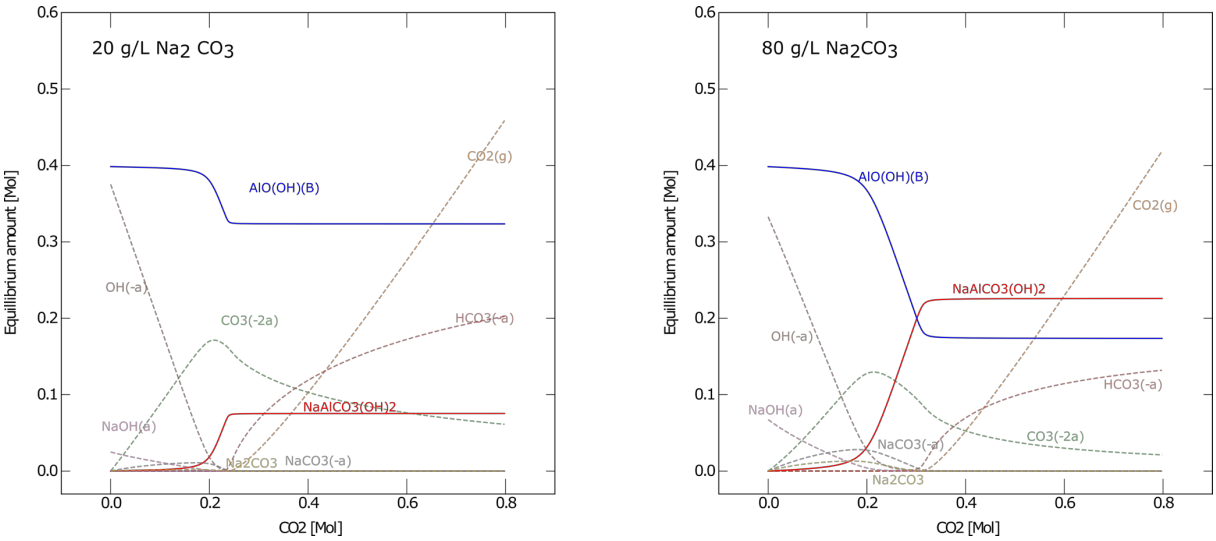

Figure 9. Equillibrium calculations of sodium aluminate solution with gradually supply of CO_2(g).

Up to 60% reduction of energy use in the calcination step can be achieved if boehmite is precipitated instead of gibbsite (Panias and Paspaliaris, 2003). Equation (5) shows the dehydration of gibbsite and Equation (6) shows the dehydration of boehmite. The enthalpy is significantly larger of gibbsite than for boehmite.

$$Al_2O_3.3H_2O = Al_2O_3 + 3H_2O \qquad \Delta H = 187 \text{ kJ/mole } Al_2O_3 \tag{5}$$

$$Al_2O_3.H_2O = Al_2O_3 + H_2O \qquad \Delta H = 72 \text{ kJ/mole } Al_2O_3 \tag{6}$$

3.3.1 Nucleation

Aluminium hydroxide can be formed from sodium aluminate solutions in a metastable zone or in an unstable zone. In both zones the solution is supersaturated with aluminium hydroxide, more material is dissolved in the solution than under normal circumstances. The degree of the supersaturation can be defined as in Equation (7) where α is the activity of the solute in the initial solution and α^0 is the activity of the solute in a solution in equilibrium. The activity can be simplified as concentration, and the supersaturation can be described as in Equation ((8).

$$S = \frac{\alpha}{\alpha^0} \tag{8}$$

$$\frac{C - C_{eq}}{C_{eq}} = S - 1 \tag{9}$$

In the metastable zone crystals are formed without self-nucleating but rather through growth or nucleation on surfaces. Nucleates are also formed homogenously in the metastable region but the size of the nucleate makes it re-dissolve immediately after created. The bulk energy of the nucleates are lower than the energy to create new solid-liquid interfaces. When a nucleate grows energy related to an interface is proportional to area of the surface and the energy related to bulk energy is proportional to the volume of the nucleate. When the rate of free energy related to volume increase faster than the interface energy nucleates grows into particles. In other words, when the supersaturation exceeds a critical concentration, homogenous nucleation appears spontaneously because the creation of interfacial surfaces does not anymore hinder growth of nucleates. The solution enters the unstable zone. If nucleates are formed on surfaces less energy intensive interfacial energies must be created. Nucleation on surfaces is called heterogeneous nucleation.

The activation energy for homogenous nucleation in the unstable zone, $S_{c,homo}$ is larger than the activation energy for heterogenous nucleation in the metastable zone that is again larger than the activation energy for growth on surfaces, $S_{c,surf}$. The activation energy for heterogenous nucleation can change for different kind of surfaces.

$$1 < S_{c,surf} < S_{c,hetero} < S_{c,homo} \tag{10}$$

The supersaturation is controlled by the critical activation limits. The critical activation limits are determined by the surface tension of the created by nucleation. The interfacial tension between aluminium hydroxide and alkaline solution is relatively high and a metastable solution can contain large amount unstable alumina hydroxide ions. Rossiter *et al.* (1998) studied homogenous nucleation in Bayer liquors. They estimated that the interfacial tension for gibbsite in Bayer liquor to be 6mJ m^{-2}. This correspond to a critical nucleation diameter for homogenous growth equal 1.2 nm. By measuring the nucleation induction period by MALLS (Multiangle light scattering) analysis the nucleation mechanism could be determined for different

supersaturations. The induction period is inversely proportional to the nucleation rate which is different from homogenous and heterogenous nucleation. They determined that homogenous nucleation appeared for S > 2.51 and S < 2.52 for heterogenous nucleation. Li *et al.*, (2013) observed that the interfacial tension increases at higher Na_2O concentration and that the interfacial tension decreases with temperature and caustic ratio (Al_2O_3 /Na_2O in solution). That means that reaching the homogenous nucleation require higher supersaturation at higher caustic concentration and lower at higher temperatures.

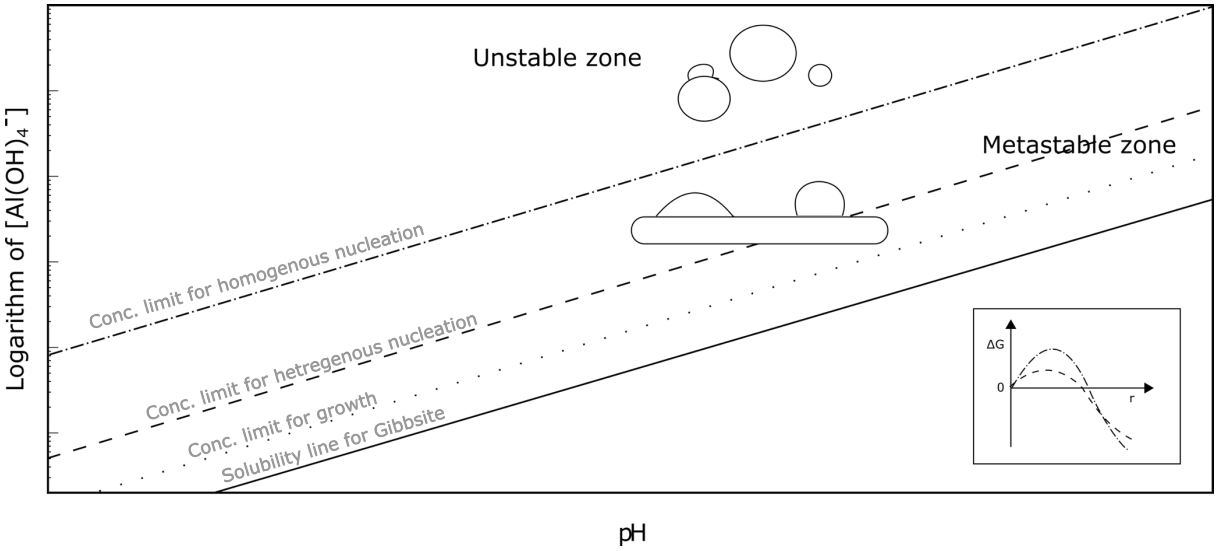

Figure 10. Solubility line of $Al(OH)_3$ and concentration limits for growth, heterogous nucleation and homogenous nuclation. The small plot in the right corner illustrates the gibbs free energy of nucleation growth (r is radius of the nuclate) for heterogenous and homogenous nucleation.

The kinetics of the precipitation is dependent on the degree of supersaturation and type of nucleation. Homogeneous nucleation creates continuously new surfaces where heterogenous precipitation and growth can occur. The increased reaction area (solid liquid interface), in addition to primary nucleation, makes precipitation from the unstable zone fast. Carbonation with CO_2 can push the system into the unstable zone by lowering the solubility of aluminum hydroxide and increasing the superasturation. The Pedersen process precipitated aluminum hydroxide for 6 hours which is fast in comparizon to the Bayer process that preform precipitation for 40-50 hours. Precipitation in the Bayer process is performed in the metastable zone as seeds are added.

3.3.2 Agglomeration and particle size

The particle size is an important characteristic for high quality metallurgical alumina. The alumina must have a certain size to sink properly in an aluminium electrolysis cell without crusting on top of the bath. This quality is referred to sandy alumina and particle diameter should be over 45 μm. Too small sized aluminium hydroxide will also lead to dust problems during calcination and during mechanically handling and carrying. Thus, large particle size, low fraction of fine particles, good mechanical strength and narrow particle size distribution is preferred for precipitated aluminium hydroxide. Crystal growth is relatively slow during precipitation and particle agglomeration is therefore the most important way to obtain desirable particle size.

Wang *et al.* (2005) studied agglomeration of particles precipitated by carbonation. They found out that the fraction of particles with diameter under > 45 μm reduces with carbonation and that agglomeration is promoted at relatively high temperature and high initial supersaturation. They claim that it is easy to obtain large particles when carbonation is used for precipitation, but it is challenging obtaining the agglomerated particles with sufficient strength.
Seeding in combination with carbonation is used in the sinter process. Zhou *et al.* (2009) obtained an average particle size of 75 μm by controlling the relative mass supersaturation; the concentration difference of aluminium species to the total content of solid in the sodium aluminate solution. Li *et al.*, (2009) managed to precipitate sandy aluminium hydroxide by introduce sodium bicarbonate, instead for carbon dioxide gas into the solution.

3.4 Silica contamination

Silica has similar behaviour as alumina in alkaline solutions. Silica follows therefor the same process route as alumina. The silicon tolerance for high quality smelter grade alumina is 0.02wt%. This tolerance leads to significant challenges for the alumina industry. The commercial Høyanger plant used low alkali concentration, 30g/L Na_2CO_3, to avoid silica impurities. Bauxite that could be used in the process was limited by the silica content. Nielsen (1978) claims that in practise the silica content in the slag should not exceed 8% when alumina content is around 44% but a slag with more alumina can tolerate higher silica content. Pedersen also mention this in his patent (Pedersen, 1927). He also mentions in the patent that small amount of free sodium hydroxide in addition to sodium carbonate lower the silica impurities.

Hollum et al. (1951) claim in their patent that the silicon impurities can be lowered by using high concentration of soda, over 70 g/L and at high temperatures, over 80°C. Leaching at temperatures over 80°C results in a sharp decrease in the silica content and at the same time an increase of the alumina content. And that this applies for any soda concentrations. At concentration above 70 g/L, the alumina extraction increases with high concentrations, but the silica concentration does not appreciably increase. Leaching at these conditions can therefore result in precipitates with lower silica content than 0.02wt%. The proposed process consists of a two-step leaching procedure. First one step with high solid to liquid ration at high temperature were not all recoverable alumina is leached. The left material from the first leaching is leached with the left liquor after the first leachate is subjected to a precipitation stage. Leaching at higher temperatures gives a higher driving force for auto precipitation as done with the Bayer process. Auto precipitation is more favourable for lowering silica content of the precipitate. Harald Pedersen mention in his patent that silica increases with total concentration of alkalis, but this might only hold for intermediate concentrations.

Longer carbonization time resulted in lower silica content for experiments related to the nepheline syenite processing (Shayanfar *et al.*, 2018). Carbonation at pH equal 11 for 2, 4, 6 and 10h had a silica content of 3.68, 1.39, 0.82 and 0.37wt%. Silicon can be removed from the aluminate solutions by adding calcium hydroxide (Noworyta, 1981). The calcium would react with silicon and form precipitates that can be separated from the solution. However, such a desilication step would increase process expenses by lower the aluminium yield and by the additional usage of CaO. Bai *et al.*, (2010) used the desilication step in the lime-soda sintering process a utilizing coal fly ash as raw material.

3.4.1 Silica for a self-disintegrating slag

A slag with too low silica concentration excludes a self-disintegrated process for size reduction after smelting. A slag with composition of at least 6% silica required no grinding after slow cooling rates (Blake *et al.*, 1966). Alpha di calcium silicate can with low cooling rate transform into its beta phase. The beta phase is necessary to transform into the gamma phase. This phase transformation experiences a volume expansion of 10% and therefor makes the slag to disintegrate by itself and facilitates slag grinding. This was also reported in the description of the Høyanger plant (Miller and Irgens, 1974). Enough silica in the slag is wanted to have full

effect of the spontaneous disintegration. This would be economical beneficial as no mechanic crushing is needed for slag size reduction.

3.5 Characterization and measuring methods

3.5.1 pH and temperature measurements

The pH measurement is done with a gel-based silver chloride glass electrode. The electrode potential is dependent on the pH of the solution. The electrode potential change can be related to pH when the pH meter is calibrated against standardised buffer solutions. The temperature can also be determined out from the same information obtained. Different error sources from pH measurement can be; contamination by precipitated species adsorbed on the electrode, contaminated calibration buffer solutions or contaminated internal solution.

3.5.2 X-ray powder diffraction (XRD)

XRD is a rapid technique for phase detection in crystalline materials in powder form. X-rays are scattered from atomic planes in crystals that produces interference effects. By changing the incident X-ray beam angle, a distinct diffraction pattern is created for the material analysed. This pattern is unique for each material and phase. Phase patterns can be found in databases and used for determining unknown phase composition by comparison. The method has limitations when it comes to detecting minor phases and determine quantitative phase composition.

3.5.3 Inductively Coupled Plasma Mass spectroscopy (ICP-MS)

ICP-MS is a method for analysing chemical composition of liquid solutions. The method can detect concentration down to as low as one part per quadrillion. Ionized atoms are separated by a mass spectrometer based on mass-to-charge ratio of ions. Light elements located right in the periodic system cannot be detected by this method. Solid material must be dissolved into a solution for be chemically analysed by ICP-MS. Constituents that does not dissolve will not be measured. This can lead inaccurate results. Highly concentrated solutions must be diluted to be analysed and the dilution makes the results obtained less accurate.

3.5.4 Laser diffraction analysis (LDA)

LDA is a technique that utilize a diffraction pattern of a laser beam passing through particle to calculate geometrical dimensions of an object. It can be used to measure particle size distribution of powders immersed in a solvent. The technique does not differentiate agglomerates from single particles, but ultrasound treatments during measurement can break up agglomerates. The technique has limitations when it comes to calculating exact size of non-spherical particles.

4 Experimental method

Chapter 4 is divided into five sections. Section 4.1 presents the working methodology and what approach the author used when embarking on the Thesis. Section 4.2 presents the characteristics of the materials used in leaching experiments. Section 4.3 presents the experimental set-up for leaching and carbonization. Section 4.4 presents how the experimental process proceeded. Here, all errors and mistakes made are explained and discussed. Partial goals for each experiment are presented as the comprehensions of the system increased throughout the process. In section 4.5, two tables of experimental conditions are presented.

4.1 Methodology

There is not much novel literature covering basic principles for precipitation by carbonation of aluminate solution or the synergies between leaching of calcium aluminates and precipitation. The author has not found any literature that describes the methods well. In addition, the practical experience for doing precipitation experiments at the laboratory used was limited. A new set-up had to be made for the experiments. On this basis, a strategy to gain as much knowledge as possible of the system was followed. An iterative process design approach was chosen. New experiment designs were based on findings from previous experiments, which enables that continuous progression throughout the work. Serious misunderstandings were made evident early in the process and improvements could be implemented. Obtaining information faster makes it possible to increase the number of iterations steps, which again makes it possible to correct more errors and misunderstanding. Characterizations techniques like XRD and LSD were preferred as these techniques were fast and could be operated by the author alone. New understandings of the system could be studied after analyzing the data from the characterization methods by designing new experiments. The ICP-MS analysis is more time consuming (as the analysis could not be done by the author alone) but the result gives indispensable information. Characterization methods like scanning electron microscopy were not done as this was estimated to be too time consuming relatively to the information gain. However, characterization by scanning electron microscopy for precipitates could give crucial information of the morphology and for nucleation mechanisms. Measuring pH and temperature are easy to implement into the experimental set-up without delaying progress. The disadvantages of the methodology used is that fewer comparative results were obtained because

the experiment conditions rapidly changed. In addition the focus on a fast progress development might have led to more inaccurate results with higher uncertainties.

4.2 Raw materials and slag characteristics

Three types of slags are used for the experiments; one synthetic slag and two real slags produced from smelting bauxite similar to the Pedersen process. The synthetic slag is used for most of the experiments.

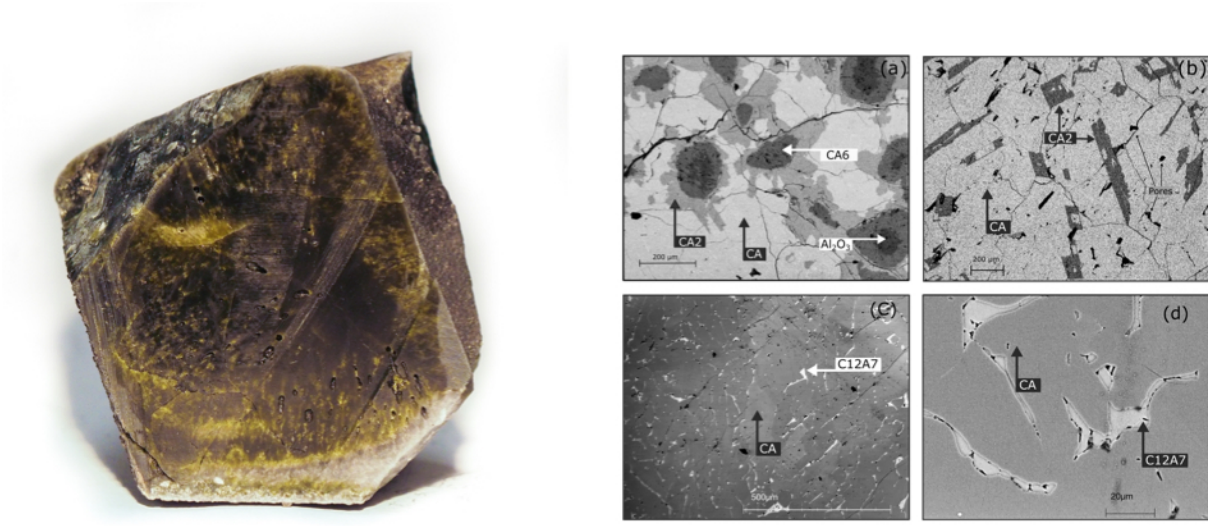

Figure 11. Left side figure: Cross section of synthetic slag. Right side figure: SEM pictures of different parts of the slag seen in left picture; (a) from the white bottom area of the slag, (b) from area between white and dark green, (c) and (d) from dark green area.

The synthetic slag was made by smelting mixed pure CaO and Al_2O_3 in an induction furnace. The complete experimental procedure and characterisation can be found in previous work (Nedkvitne, 2018). Left picture in Figure 11 shows a cross-section of bulk material separated from the crucible. The right pictures in Figure 11 present scanning electron microscop images of different parts of the slag. The slag consist of krotite (CA) and small amounts of mayneite (C12A7). There is also traces of grosite (CA2) that originates from slowly reacted alumina located at the bottom part of the crucible. The white area in left picture of Figure 11 consits of grossite in a krotite matrix. The syntetic slag was crushed in a planetary mill and mixed in an automatic powder mixer to ensure homogenuity. The calcium alumina ratio in the slag was found by ICP-MS analysis. Powder was digested into strong acid and the aluminium and calcium concentration could be determined from the solution.

Figure 12. Real slags produced from bauxite.

The two real slags are named RS1 and RS2. A picture of bulk and final powder of the two slags is shown in Figure 12. RS1 is made in a pilot scale bauxite smelting experiment. The slag self-integrated by time and no milling was needed to obtain leachable powder. The left picture of RS1 in Figure 12 shows the bulk material that primarily consisted of granules that disintegrated with weak mechanically handling. Hard granules that could not be crushed by hand were removed. Pieces of metallic iron was separated out with a strong magnet.

Table 2. Slag characteristics.

Slag	Chemical compostion [wt%]					Phase composition	Mean Particle size	Self disintegrated
	Al_2O_3	CaO	SiO_2	TiO_2	Fe_2O_3			
RS1	36,3	57,9	2,8	0,89	0,82	C3A and C12A7	115µm	Yes
RS2	46,1	48,1	2,3	1,8	0,44	C12A7 and CA	45µm	No

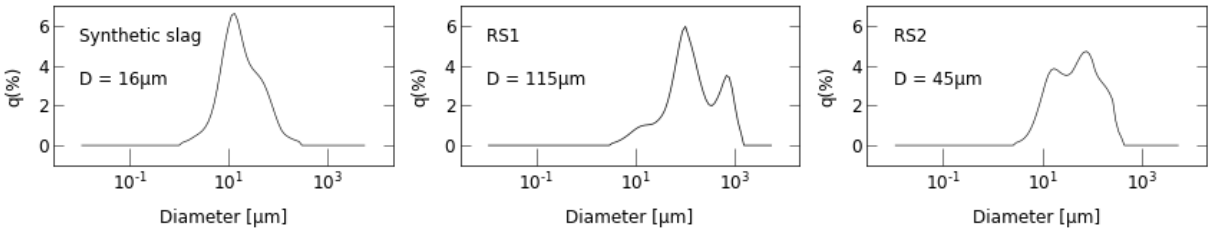

Figure 13. Particle size distribution of slags.

The slags are drawn into the $CaO\text{-}Al_2O_3$ and the $CaO\text{-}Al_2O_3\text{-}SiO_2$ phase diagram (see Figure 14). The location is based on the chemical analysis of the three slags and the phase composition in the phase diagram correlates good with XRD analysis.

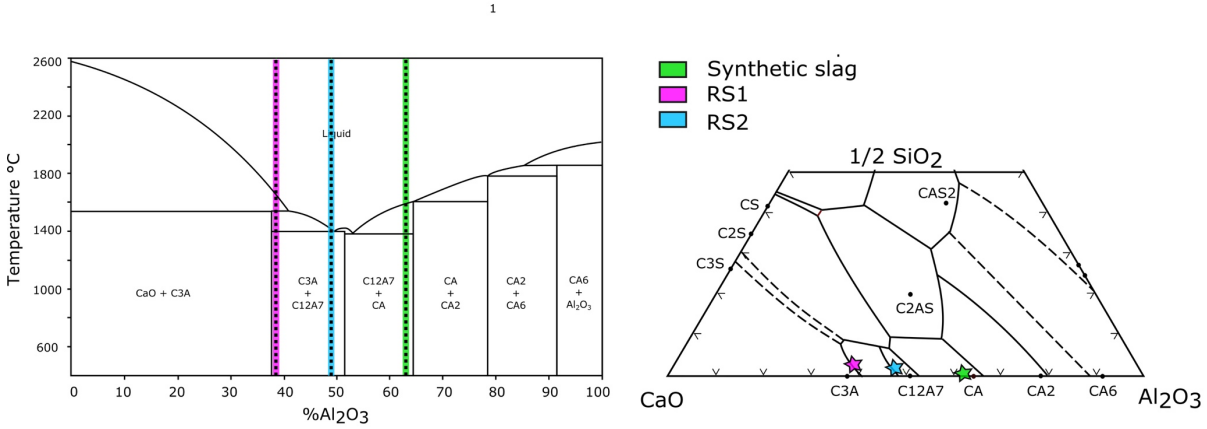

Figure 14. The three slag placed in the binary CaO-Al_2O_3 phase diagram and thernary CaO-Al_2O_3-SiO_2 phase diagram.

RS2 originates from small-scale lab experiments studying low-grade bauxite smelting. The slag was hard and solid, and no sign of a (preferred) self-disintegration process was observed. The left picture of RS2 in Figure 12 shows granules of the slag that was crushed to powder (see right picture) in a planetary mill. Chemical composition, phases in the slag and mean particle size of the two slags is listed in Table 2. Chemical analysis was performed with XRF from studies of the slag makings.

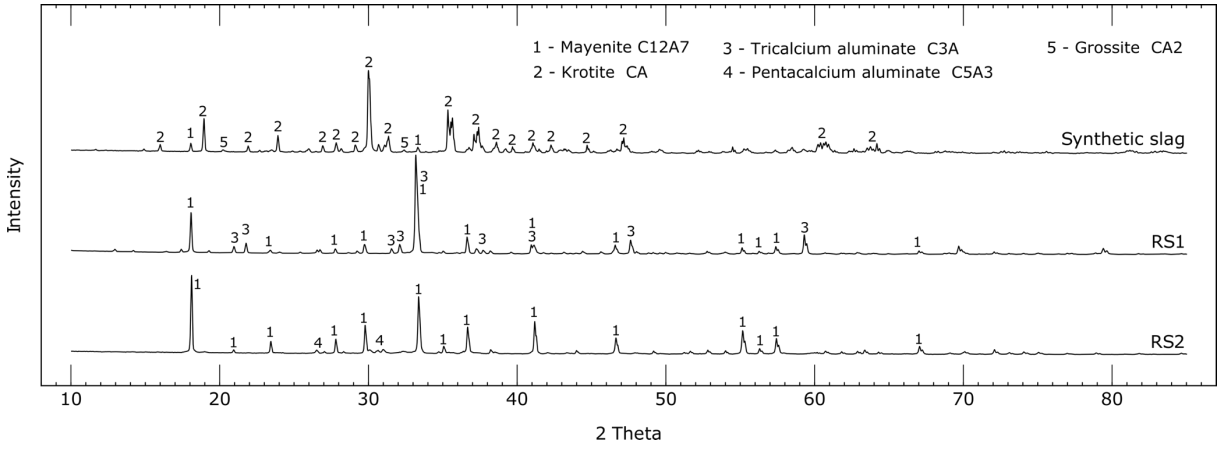

Figure 15. XRD patterns of slags

XRD patterns of all three phases can be found in Figure 15. The most distinctive peaks for the synthetic slag, RS1 and RS2 represent Krotite (CA), Tricalcium aluminate (C3A) and Mayenite (C12A7). No calcium silica phases can be seen in the XRD patterns for RS1 even though small parts of the phases must exist because of the self-disintegration process. Particle size distribution analysis done by LDA can be found in Figure 13. The synthetic slag has very small

particle size with a narrow distribution. Larges fraction of the particles in self-disintegrated slag (RS1) consist around 100+50 micro meter, but also a larger fraction of particles around 700+-150. The particle size distribution of this slag is determined by how calcium silicate phases are distributed in the slag. RS2 has a wider particle size distribution and lager particles than the synthetic slag.

4.3 Experimental setup

4.3.1 Set-up for leaching experiments

Leaching experiments were executed with a simple set-up and all experiments followed the same procedure. Beakers containing the distilled water were placed on top of a hotplate with magnetic stirring. Sodium carbonate were mixed with distilled water and heated to desired temperature. Temperature were controlled with a thermocouple immersed in the liquor that is connected to a hot-plate. Thenceforth the slags were immersed into the solution and leached for 1 hour. The beakers were covered with Parafilm to reduce evaporation. The pH and temperature were measured with a silver chloride electrode throughout leaching. Figure 16 illustrates the set-up. The leaching grey muds were filtered out in a Buchner Funnel with filtration paper assisted by a simple vacuum pump.

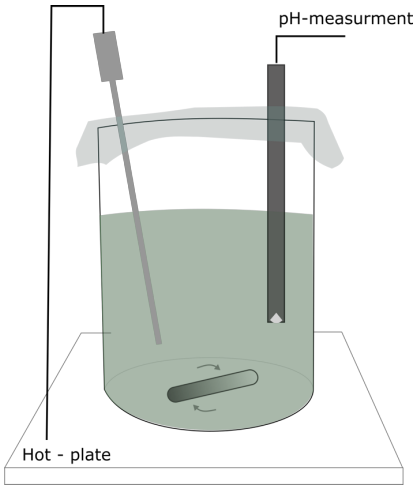

Figure 16. Experimental set-up for leaching.

4.3.2 Set-up for precipitation experiments

The precipitation experiments were executed on a plate with magnetic stirring. The liquors were cooled down towards room temperature after leaching. Temperature were not controlled befor carbonation start. Carbon dioxide gas were introduced to the solutions through a purging stone and the pH was measured during carbonation. When the pH reached certain values, carbonations were stopped. The liquors were left with slow agitation for further precipitation overnight and filtered and dried approximately 20h after the carbonation. Several improvements of the set-up were implemented throughout the work. Gas flow meters were connected to an argon and carbon dioxide bottle to control the partial pressure and flow of carbon dioxide gas. The purging stone had to be changed to a pipette tip due to clogging that resulted in dysfunctional gas flow meters. The set-up is illustrated in Figure 17.

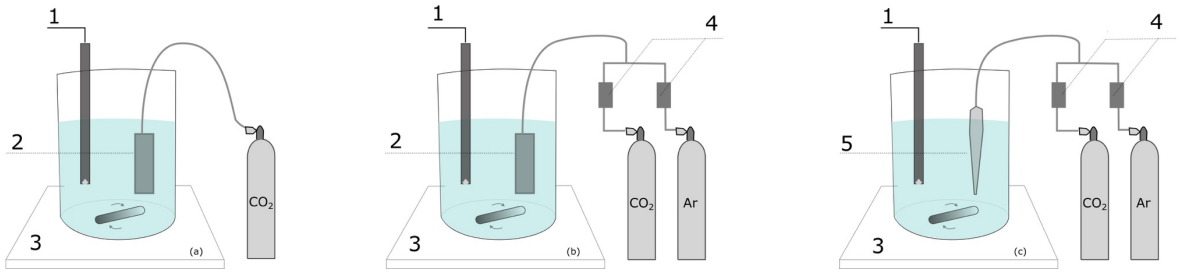

Figure 17. The development of experimental set-up for precipitation from left to right. Experiment C and all D experiments used the left setup (C without magnetic stirring). All E, F1 and experiment F2 used the setup illustrated in the middle. F3, G and all H experiments used the setup illustrated to the right. 1: pH meter, 2: purging stone, 3: magnetic stirring plate, 4: gas flow meters, 5: pipette tip.

4.4 Experiments performed

All experiments preformed are noted with a letter following the alphabet in chronological order. An overview of the experiments can be found in tables in Chapter 4.5. where the experimental conditions are presented. The motivation for choosing experimental conditions changed throughout the working period. The decisions for changing experimental set-up or conditions are explained in the following chapter. Adjustments were implemented as results of errors or the discovery of relevant literature.

The aim for the preliminary experiments were to explore how solid to liquor ratio effects aluminium extraction at low and high temperatures and how this effected precipitation by carbonation. Literature found for leaching experiments of calcium aluminates had higher solid

to liquid ratio than used in the Pedersen process (Tong and Li, 2008). This could be interesting for a possible high efficiency version of Pedersen process using high alkali concentration and large solid to liquid ratio. Higher solid to liquid ratio leads to less tank volume and can be beneficial for an industrial process. Three experiments (A1, A2 and A3) were carried out at 80°C and three at 40°C degrees (B1, B2 and B3). The solid to liquid ratio were 1:5.5, 1:7 and 1:10 for both temperatures. Sodium carbonate was mixed with 200mL of distilled water to obtain a 100g /L Na_2CO_3 solutions. pH was measured during leaching. The leachates were stored in plastic containers for later precipitation experiments. Auto precipitation started during storage and the leachates were determined to be unsuitable for further precipitation experiments and chemical analysis with ICP-MS. After about two months with storage, the auto precipitates were analysed with XRD and the rest liquors by ICP-MS.

An unsuccessful experiment was carried out before the A and B experiments testing a 1:3 liquid to solid ratio. The experiment was aborted due to e.g. insufficient mixing and water absorption. The solid was re-leached at 60°C for over 90 minutes adding more water and sodium carbonate to the solution. The leachate, approximately 250mL, was used to perform the first precipitation experiment, noted C in Table 4. Pure carbon dioxide gas was introduced to the leachate via a stainless-steel purging stone with 0.5µm pore size. The gas flow rate was not precisely controlled. The pH and temperature were continuously measured until the pH was equal 9. Then the precipitate was filtrated (as far as it was possible as it had a gel like structure), dried, crushed and analysed with XRD.

The precipitate did not have right composition in the first precipitation experiment C (see XRD results in section 5.2.). The author decided lower the alkali concentration and reduce the degree of carbonation with thoughts of avoiding unwanted precipitation phase. Leaching experiments were performed with 30 g Na_2CO_3/L at 45°C with a 1:10 solid to liquid ration. A larger batch, 400 mL of water, was leached in order to obtain enough leachate for several precipitation experiments. Due to a defect pH meter electrode, the precipitation with CO_2 was delayed one day. Auto precipitate formed during night was characterized with XRD. The leachate was split into 4 samples, 75mL each, after the material precipitated during night was filtered out. The carbonization was stopped at different pH for each sample with a pH meter that did not have logging features. The pH was therefore not continuously measured. The precipitate was filtered out, dried and analysed. Samples for ICP-MS was taken out and diluted with distilled water. The purpose of the author was to avoid auto precipitation during storage. This was of course

not the case as the aluminium hydroxide solubility is function of alkali concentration. Precipitates were also observed in these samples. In total no chemical analysis could be performed for the A1-3, B1-3 and D experiments.

After conducted equilibrium calculations (see theory section) for the precipitation system at different alkali concentrations and the discovery of M. Hollum *et al's*, (1951) patent, the author decided to again focus on experiments analysing precipitation from solutions with high alkali concentration. Gas flow meters were installed for mixing CO_2 gas and argon as illustrated in Figure 17. Subsequently the CO_2 partial pressure and flow could be controlled. The aim was to obtain a less aggressive carbonizing gas and avoid wrong precipitate phase composition. Two batches, E and F, with 650 mL of water, 100g/L Na_2CO_3, 1:10 slag to liquid ratio at 85°C were leached for one hour. The batches were split into 3 smaller potions and carbonized with different CO_2 flow and partial pressure. The gas flow meter failed several times due to a clogging purging stone during precipitation. Therefore, the purging stone was changed with a pipette tip for the last experiment F3. The ICP-MS samples of pregnant solutions after leaching were mixed with a NaOH solution of known concentration. The leachate concentrations could then be calculated back from the ICP-MS results. No auto precipitation was observed in these samples.

The following experiments were used to conduct leaching and precipitation experiments on real slags with the intension of study silica contamination. The author wanted to study similar systems as M. Hollum *et al*, (1951) presented. They claimed that the silicon concentration in the solution drastically changed around 70°C. The solubility of silica could not abruptly decrease due to the silica solubility and the author of this Thesis wanted to check if a structure change of the grey mud could lead to low silica in solution and high in the grey mud. Only one experiment was carried out with RS1. The author decided to try this slag as it had the right self-disintegration characteristics and a higher silicon content. The decision of not carry out more experiment with the slag was taken after XRD analysis of the grey mud and the observance of a low supersaturated solution during carbonation. The slag seemed not preferable with respect to leachability. Three experiments, H1-3, were carried out with RS2 with the intension of checking the effect of leaching temperature on silicon contamination. Temperatures equal 50°C, 70°C and 90°C were used for leaching and the same carbonization conditions were used for all three experiments. Unfortunately, was the ICP-MS sampling after leaching for H2 missed

out. The precipitates were dissolved in highly concentrated NaOH solution to check the final silicon impurity level of the precipitate with ICP-MS.

4.5 Experiment conditions

The experimental conditions for leaching are listed in Table 3 and the experimental condition for carbonation are listed in Table 4.

Table 3 Parameters for leaching experiments.

Experiment	Volume [mL H2O]	Slag	Solid to liquid ratio	Mass slag [g]	Alkali concentration [g Na_2CO_3/L H_2O]	Temperature [°C]
A1	200	Sythetic	1:10	22,0	100	80
A2	200	Sythetic	1:7	31,4	100	80
A3	200	Sythetic	1:5.5	40,0	100	80
B1	200	Sythetic	1:10	22,0	100	40
B2	200	Sythetic	1:7	31,4	100	40
B3	200	Sythetic	1:5.5	40,0	100	40
D	400	Sythetic	1:10	40,0	30	45
E	650	Sythetic	1:10	65,0	100	85
F	650	Sythetic	1:10	65,0	100	85
G	200	RS1	1:7	28,6	100	90
H1	200	RS2	1:7	28,6	100	90
H2	200	RS2	1:7	28,6	100	70
H3	200	RS2	1:7	28,6	100	50

Rotation speed was adjusted to the total volume of the leachate. For leaching the 200mL solution 350rpm were used.

Table 4. Parameters for precipitation experiments.

Experiment	Volume [mL]	Continously pH measuremnt	Stopped purging [pH]	Controlled gas flow [slpm][1]	Reduced CO_2 partial pressure	Gas inlet
C	250	Yes	9.8	No	No	Purging stone
D1	75	No	12.9	No	No	Purging stone
D2	75	No	12.67	No	No	Purging stone
D3	75	No	12.15	No	No	Purging stone
D4	75	No	11.5	No	No	Purging stone
E1	160	Yes	12.57	Some[2]	Some[2]	Purging stone
E2	160	Yes	12.171	Yes	Yes, 0.3	Purging stone
E3	160	Yes	12.278	Yes	Yes, 0.7	Purging stone
F1	145	Yes	12.25	Some[2]	Some[2]	Purging stone
F2	145	Yes	11.8	No[2]	No[2]	Purging stone
F3	145	Yes	11.98	Yes	Yes, 0.5	Pipette tip
G	155	Yes	11.5	Yes, 1.5	Yes, 0.33	Pipette tip
H1	130	Yes	11.72	Yes, 1.5	Yes, 0.33	Pipette tip
H2	170	Yes	11.49	Yes, 1.5	Yes, 0.33	Pipette tip
H3	179	Yes	11.49	Yes, 1.5	Yes, 0.33	Pipette tip

[1] Standard liter per minute

[2] Failing gas flow meter

5 Results

The chapter is divided into subsections presenting results obtained from the different characterisation or measuring techniques from leaching (Section 5.1) and from precipitation (Section 5.2.). The chemical analysis of solutions and precipitates are presented in Section 5.3. All data processing and visualisation is done with Matplotlib and Pandas packages in Python.

5.1 Leaching results

5.1.1 pH and temperature measurements

The pH measurements from all experiments are shown in Figure 18. The pH is higher for leaching at lower temperatures (B1-3 and H3). The pH is lower on the experiment were lower alkali concentration was used (D).

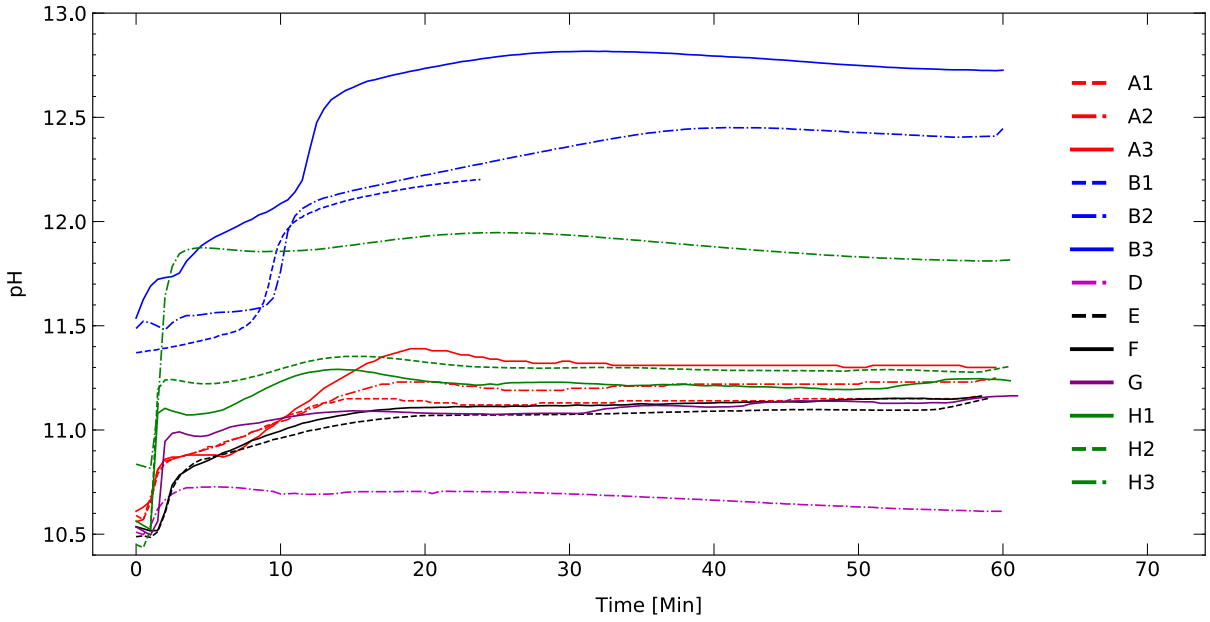

Figure 18. pH measurments during leaching experiments.

The pH measurement for B1 was unsuccessful. New settings on pH measurements made the logging stop after a short period of time. The pH measurement curves have about similar shapes. The pH immediately increases when the slag is immersed into the solution. However, this increase was not observed before about 10 minutes for B experiments. This first increase more intense at lower temperatures as seen in experiment H1-3 where only temperature is changed. After the increase the pH flattens out or decrease for a few minutes for experiments done with

a high solid to liquid ratio (H1-3, G, A3). The experiment that experienced decrease for longest time was the experiment with highest liquid to solid ration (A3). The pH increases then to a high point before it stabilizes. The high point shifts towards the right at lower temperature. This can clearly be observed for experiment H1-3. Some experiments experience a small decrease before it stabilizes. The experiments with lowest total volume, H1-3 and A1-3 (200mL) have sharper changes in pH compare to the larger batch experiments, E and F (650mL).

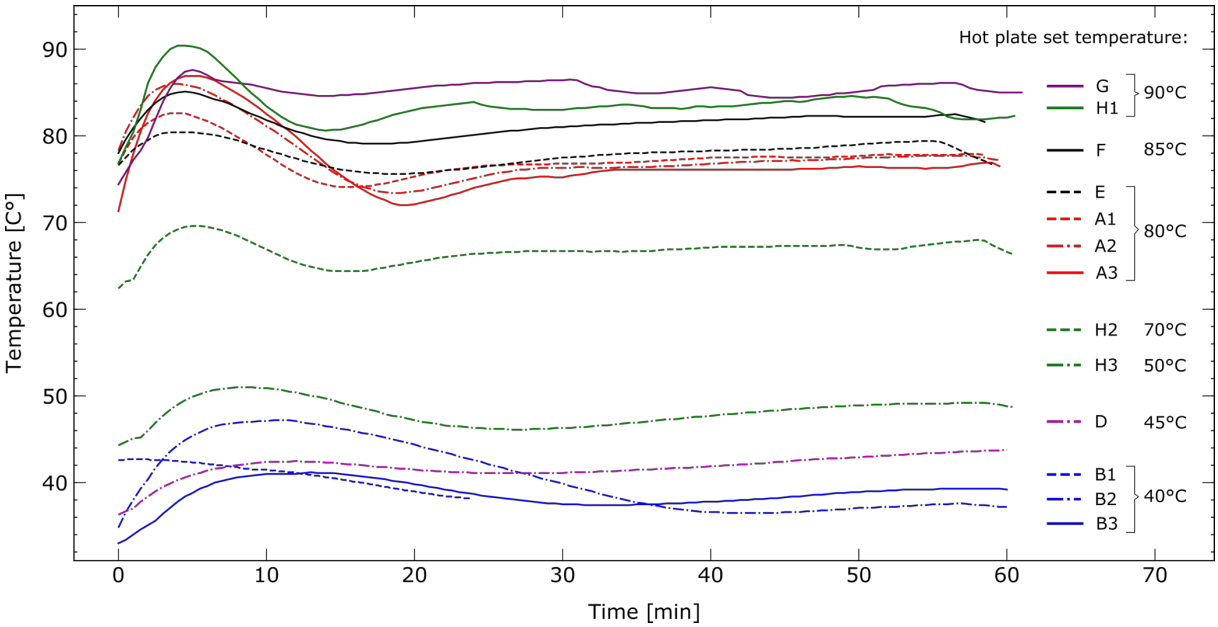

Figure 19. Temperature measurements during leaching experiments.

The corresponding temperature measurements are presented in Figure 19. The temperature increases when the slags are immersed into the solution. Peak temperatures are observed after 5-10 minutes, a bit before for leaching at higher temperatures. The temperature decreases before it rises to a stable temperature. The temperature peak is broader for leaching experiments done at lower temperatures. The set temperature on the hot-plate deviates significantly from measured temperature, which indicate inaccurate temperature measurements. However, important information can be retrieved by compere temperature curves from different experiments and see how temperature develops throughout leaching.

5.1.2 Grey mud characteristics

All grey mud formed absorbed water. By applying shear stress (agitation) to the filtrates, a substantial more amount of liquor could still be extracted when the vacuum pump could not suck out more liquor. The loss of liquor was higher for leaching experiment preformed at high

solid to liquid ratio and for experiment preformed at higher temperatures. The loss varied from approximately 10 to 55%. Some of the loss originated from evaporation.

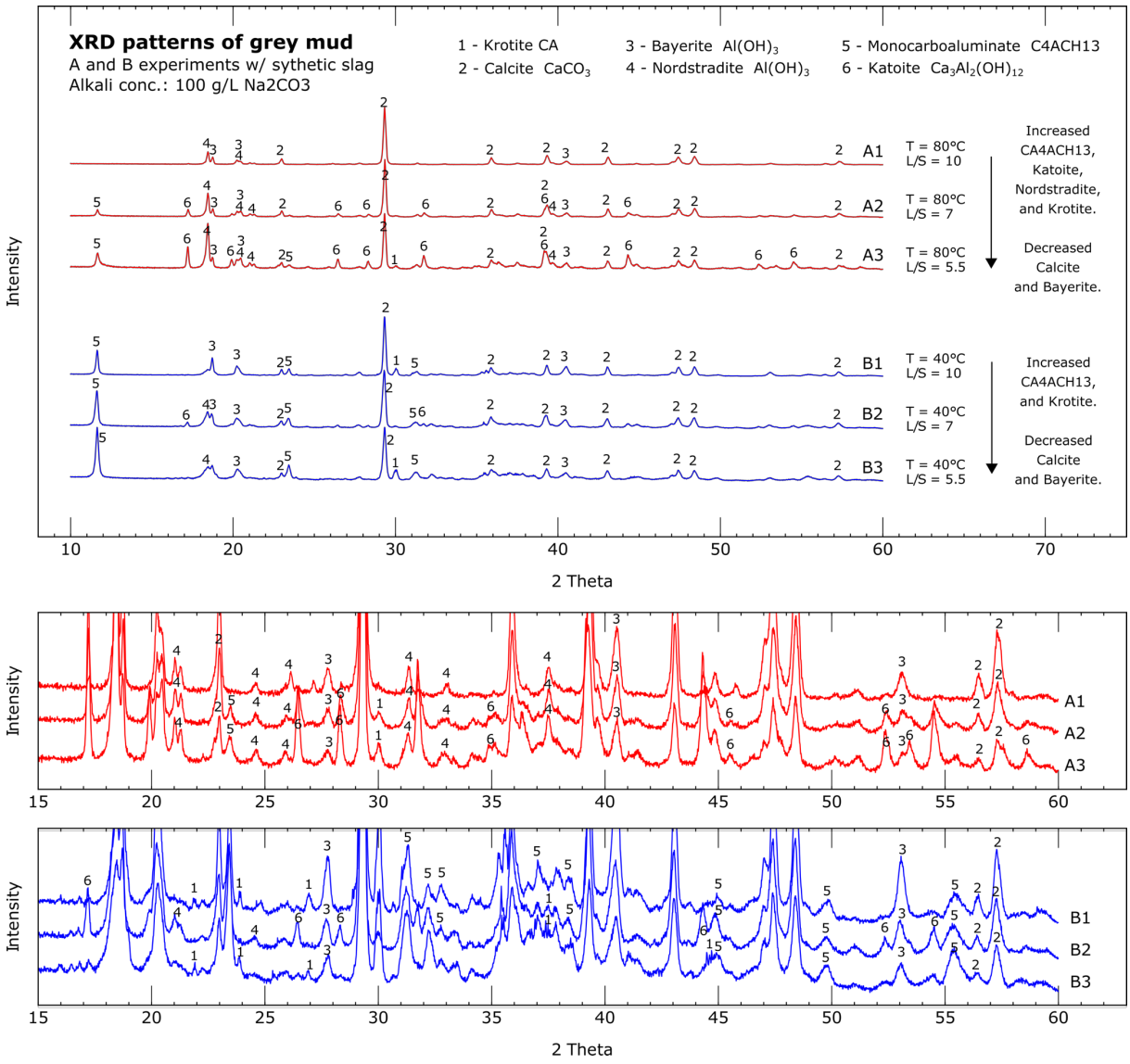

Figure 20. XRD patterns of grey mud from experiment A1-3 and B1-3.

XRD patterns for grey mud from experiments A and B can be found in Figure 20. The most intensive peak for all XRD patterns comes from $CaCO_3$. The second largest highest peaks in all B experiments comes from monocarboaluminate. The phase, $Ca_4Al_2(CO_3)(OH)_{12}(H_2O)_5$, has the cement chemical notation CA4ACH13. This phase is also observed in combination with Katoite, $Ca_3Al_2(OH)_2$, in A2 and A3 experiments. At low temperature, indicated with blue colour in the XRD pattern, can we find unreacted krotite (CA) for experiments with the highest and lowest solid to liquid ratio (B1 and B3). See peak at $2\theta = 30$ for blue coloured XRD pattern. In experiment B2 no krotite is found, but instead katoite (see peak $2\theta = 17.2$ blue patterns).

This cannot be found in the grey mud from B1 and B3 where krotite are found. katoite is abundant for experiments done at high temperatures (XRD with high liquid to solid ratio (A2 and A3). The peaks at 2θ = 17.2 and 2θ = 52.5 shows that the grey mud consist of larger fraction of kaotite at higher liquid to solid ratio. The XRD peaks for unreacted Krotite is also very low for these experiments. For the experiment at high temperature with low fraction of solid (A1) no XRD peaks for unreacted krotite, katoite or monocarboaluminate can be found. Grey mud with kaotite also have large amounts of the aluminium hydroxide polymorph Nordstrandite. Grey mud from experiment A1 and B3 has Nordstrandite without having peaks for Kaotite but the intensity of the peaks is lower. The amounts of the aluminium hydroxide polymorph Bayerite are lower for higher solid to liquid ratio for low and high temperatures (see peak 2θ = 27.8).

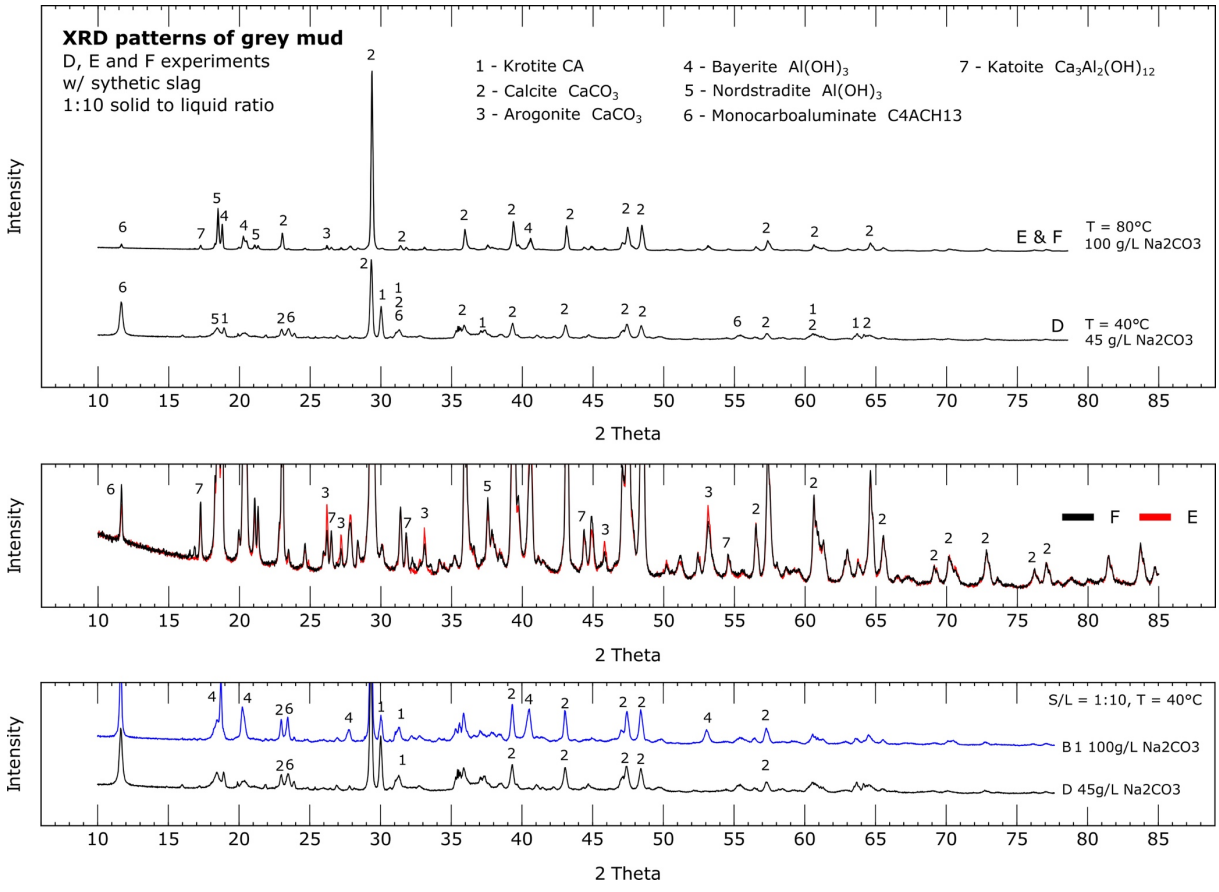

Figure 21. XRD pattern of grey mud from the E, D and F experiments.

Monocarboaluminate also appears in the grey mud for experiment D where leaching is done at low temperature and low and low alkali concentration. Experiment B1 and D is performed at same condition except the alkali concentration. Bayerite appears on the XRD patterns for B1

which is leached at 100g/L Na_2CO_3 compared to 45g/L Na_2CO_3 in experiment D. The peaks for unreacted krotite is also less intense than in D. Experiment F and E are done under same conditions and the XRD pattern of the grey mud is similar (some more aragonite in experiment E). In the other hand, experiment A1 is also done under the same conditions with the exception a smaller scale and higher stirring speed. A1 have no peaks representing monocarboaluminate, katoite, krotite or aragonite in the grey mud XRD pattern.

Summarized findings of structures of grey mud originating form leaching of synthetic slag:

- More unreacted slag (krotite) in grey mud from low temperature experiments. Even more unreacted slag for low concentration experiments.
- Grey mud form experiments with a higher solid to liquid ration constitute of more complex hydrated compounds and nordstrandite and less calcium carbonates and bayerite. Lower temperatures favouriting monocarbonaluminate formation and higher temperatures katoite.
- More bayerite is found in grey mud from experiments done at higher sodium carbonate concentration.
- More intense agitation leads to less katoite or monocarbonaluminate and more unreacted krotite.

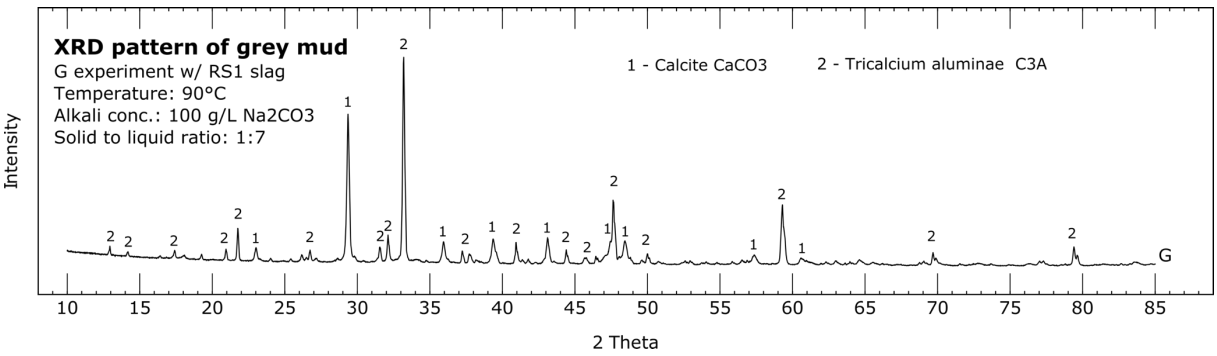

Figure 22. XRD pattern of grey mud from G experiment.

The grey mud from experiment G constitute of calcite and unreacted slag (see Figure 22). The main peak for unreacted slag is higher than the highest peak for calcite.

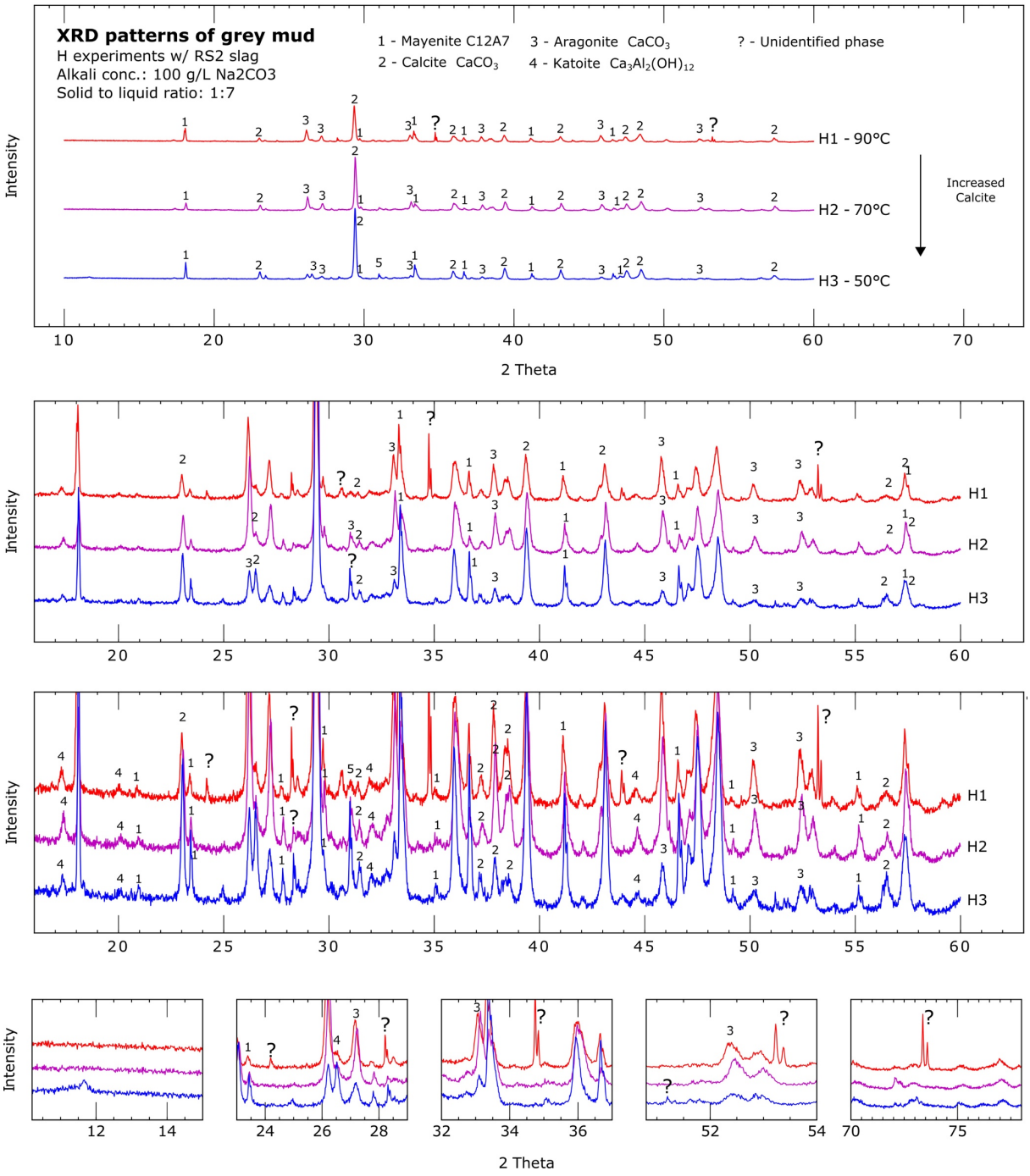

Figure 23. XRD pattern of grey mud from H1-3 experiments.

The grey mud patterns of experiment H1-3 are very complex. The grey mud consists of many phases making it difficult to identify every diffraction peak. The main phases identified are unreacted mayenite C12A7 and the two $CaCO_3$ polymorphs calcite and aragonite. Other main findings are summarized below.

- There are less calcite in the experiment preformed at higher temperatures.
- Equal amount of aragonite is found in experiment preformed at 70°C and 90°C. More than the experiment at 50°C.
- More aayenite is found in lower temperature experiments.
- A distinctive unidentified phase is found in experiment H1 (90°C). Peaks at two theta equal 24.2, 28.3, 34.7, 44, 53.3 and 73.5. The phase could not be identified with the pdf database.
- Small amount of Katoite is found in all experiments.
- An unidentified peak is found in H3 at two theta equal 11.8 and 31.
- Unidentified phase in all three grey muds at two theta equal 28.4.

5.2 Precipitation results

No precipitation was observed during the first part of carbonation. The precipitation started at different time depending on the experiment. The solution turned white when enough precipitates had formed. The transition from transparent to white appeared faster for some experiment than others.

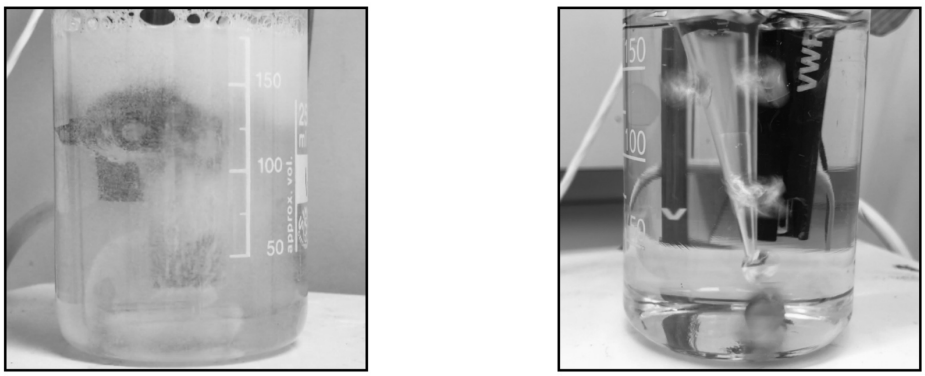

Figure 24. Pictures of carbonization set-up with purging stone and pipette tip.

The CO_2 bubbles from the purging stone is much smaller than the bubbles from the pip pipette tip set-up making a much large total gas-liquid interface. The top of the beaker has a larger tendency to foam than the set-up with the purging stone.

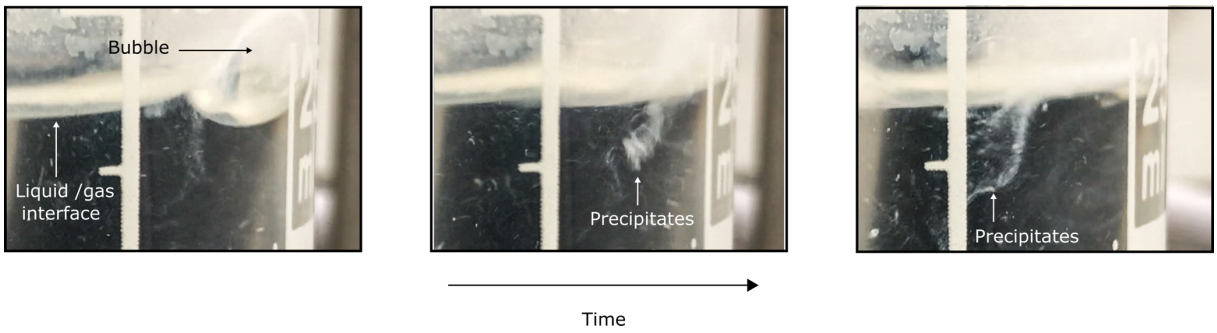

Figure 25. Precipitation at the gas liquid interface. pH 12.1 at 30 min carbonation. H2 experiment.

Precipitation clusters originating from bubbles bursting at the solution surface were observed with experiments done with a pipette tip set-up. Figure 25 showing three images capturing one occurrence. This form of precipitation was more frequently observed longer out during carbonation.

5.2.1 Carbonation measurements

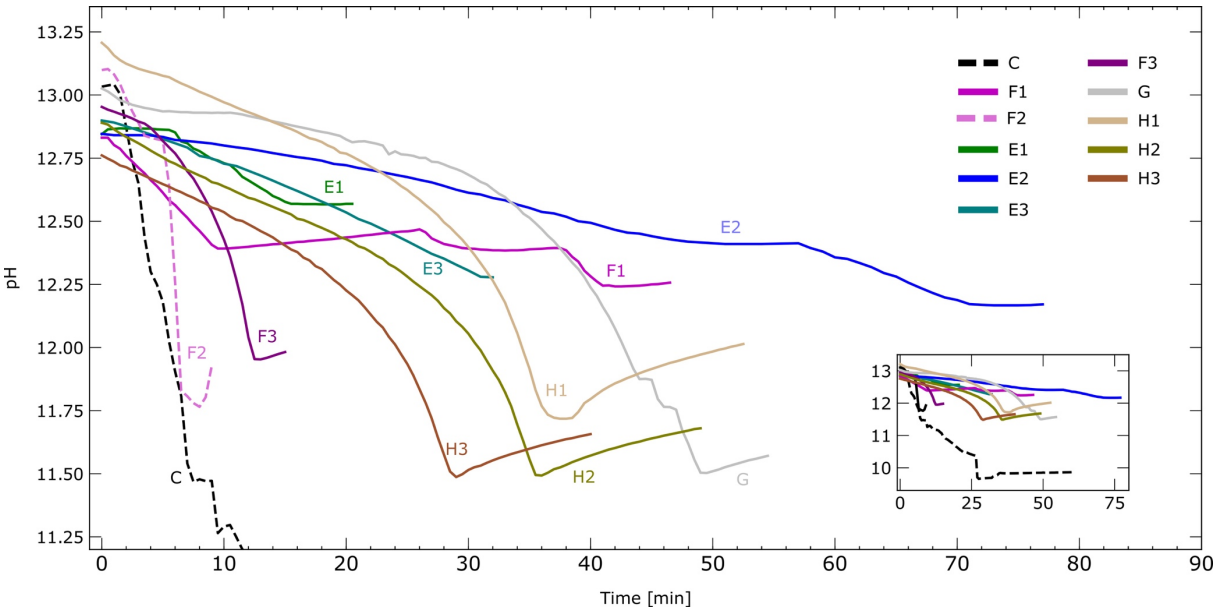

Figure 26. pH measurements during carbonization.

As mention before, pH was measured for all carbonations except the D experiments as the pH meter was dysfunctional. All measured pH curves can be seen in Figure 26. The failing gas flow meters resulting from clogged purging stones can be seen in the pH curves as sharp bends. When the gas flow meter controlling the CO_2 stopped working a sudden increase or a flattening

curve can be observed at the pH curves. This applies for experiment E1, E2 and F1. In experiment F2 the gas flow meter controlling the argon gas stopped resulting in purging of pure CO_2 gas. The pH drops with a rate up to 0.13 per minute.

Experiment F3, G, H1-3 were done with the pipette tip set-up and experiment G and H1-3 had all same agitation speed. The curves for these experiments have similar shapes. A constant pH change in the start transforms into more and more pH decline. The decline rate stabilizes before the carbonations were stopped. In experiment H1, and somewhat in experiment H3, the pH rate increases after stabilizing. The pH rises immediately after carbonation stop, first with increasing pH rate, then with more constant rate (slightly exponentially decreasing). The rise of pH was noticed for that last precipitation experiments the pH measurement was continued for about 10-15 minutes after carbonation stop for these experiments.

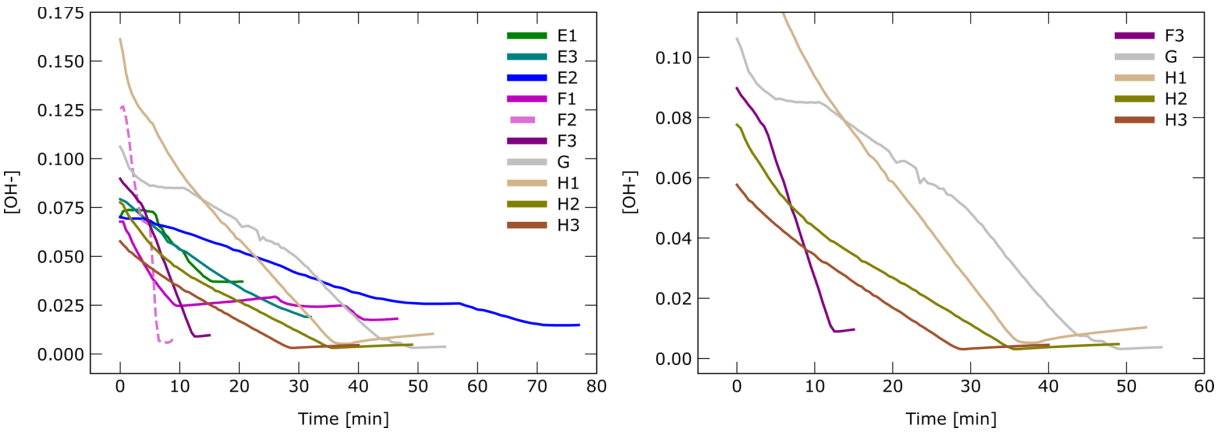

Figure 27. pH measurements calculated to [OH^-].

The hydroxide ion concentration can be calculated when the pH is known. Figure 27 presents the pH plots as hydroxide concentration. The hydroxide concentration decreasing linearly, or slightly decreasing until carbonation stops as seen in the derivative plot (second from left) in Figure 28. Then the hydroxide concentration increases linearly, or slightly decreasing when seen at the far-right plot in Figure 28. Hydroxide ions are important reactants and products during carbonation and precipitation.

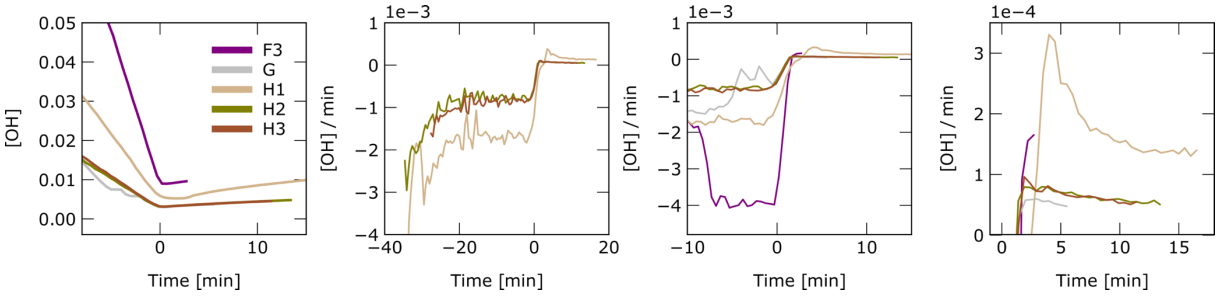

Figure 28. Hydroxide ion concentration versus time normalized to carbonation stop. From left to right; hydroxide ion concentration, rate of hydroxide ion concentration changes during carbonization, rate of hydroxide ion concentration changes near carbonization stop and rate of hydroxide ion concentration change after concentration stop.

Temperatures measured are plotted Figure 29. The solutions left after leaching were cooled to around room temperature down before the carbonation starts. The cooldowns were not exactly controlled and starts carbonations at slightly different temperatures. Experiments with high carbonation rates have a larger temperature increase and experiment with a low carbonation rate have a slow temperature increase. Most temperature curves have first an increase in temperature to a high point before it decrease at slightly slower rate. When carbonation stops the temperatures are decreasing linearly. The right plot in Figure 29 shows the experiments with same carbonation conditions. Experiment G has larger decrease in temperature than H1-3. Experiment F3 has a larger increase in temperature than H1-3.

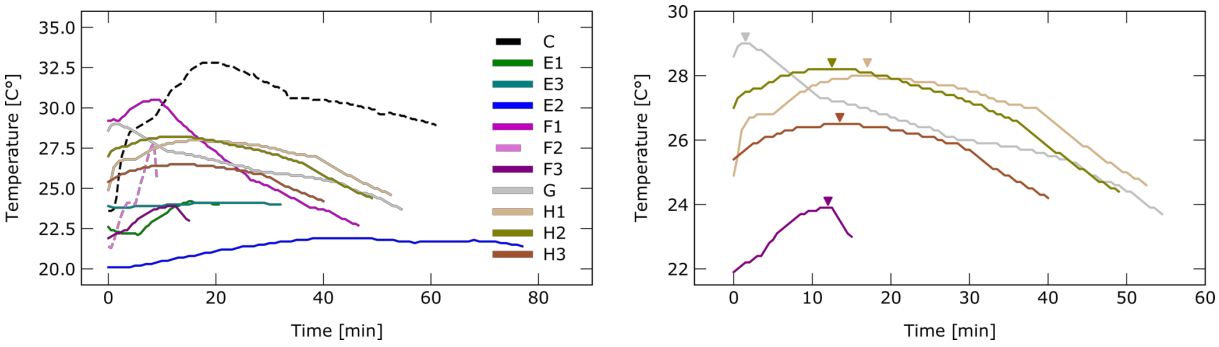

Figure 29. Temperature measurements during carbonization. The mark indicates global maxima temperatures.

5.2.2 Phase composition

All carbonation experiment except C, D4 and F2 precipitated out aluminium tri hydroxide. The XRD patterns of the precipitates are presented in Figure 30. All precipitates constitute of the

$Al(OH)_3$ polymorph Bayerite. D3 and H1 also have XRD peaks for the $Al(OH)_3$ polymorph Gibbsite that are significant. Peak representing Gibbsite can also be seen in F1, F3 and E1.

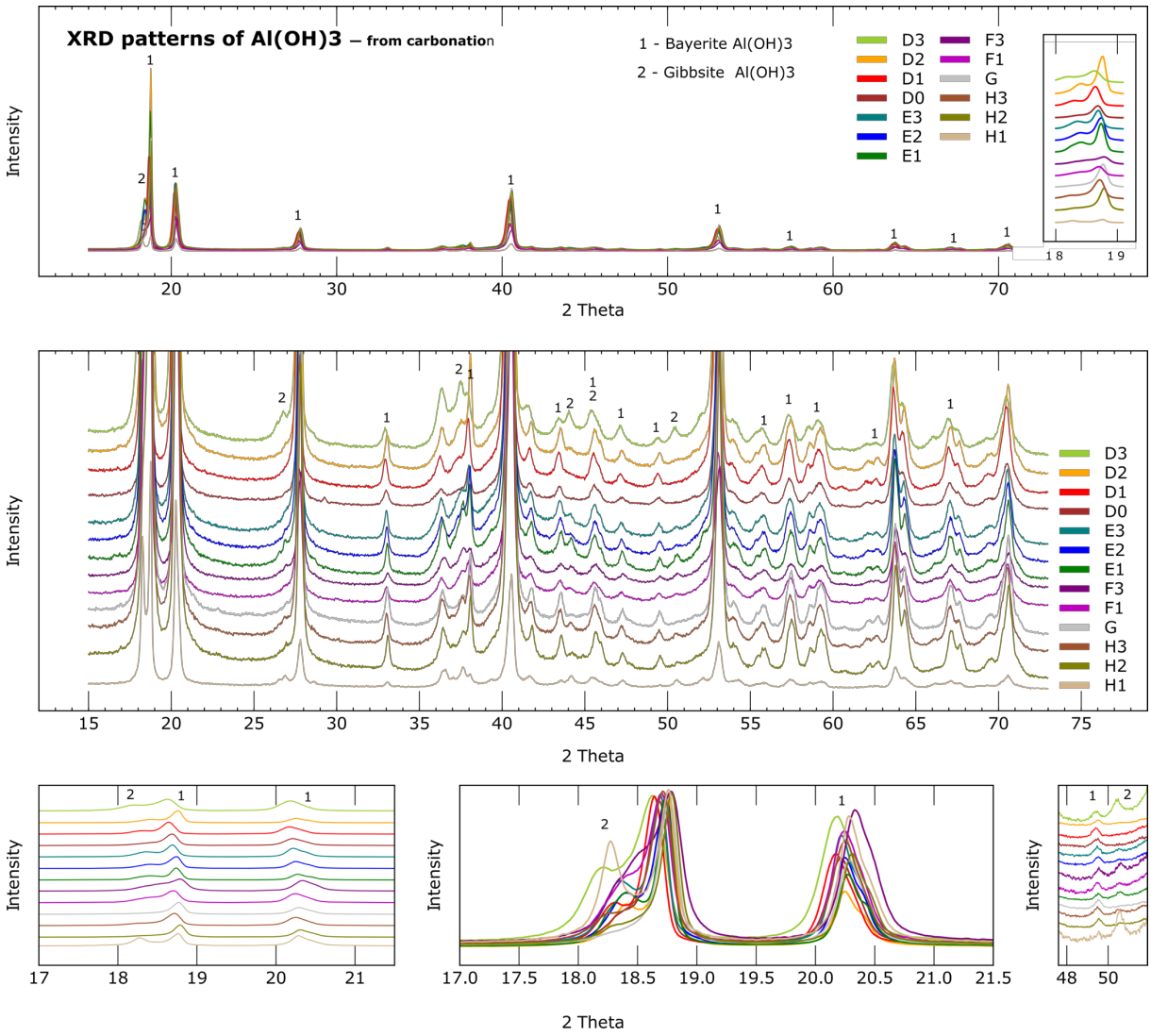

Figure 30. XRD patterns of precipitates consisting of aluminium tri hydrate. The upper right plot in the upper plot illustrates the intensity of XRD raw data. In the three lower plots, XRD patterns are normalized to the highest peak so the amount of Bayerite and Gibbsite are easier to compare.

XRD analysis were also taken on the precipitates in sample A1-3 and B1-3. These samples did not get any carbonation treatment. Precipitate from experiment B3 contains only bayerite and from experiment A3 contains primarily gibbsite. More Bayerite compared to gibbsite are formed at lower supersaturation, lower liquid to solid ratio, except for B3. The precipitation from B3 seemed to originate only from spontaneously precipitation and the precipitate from A1 originated only from growth on the container wall. The other from both homogenous and heterogenous nucleation.

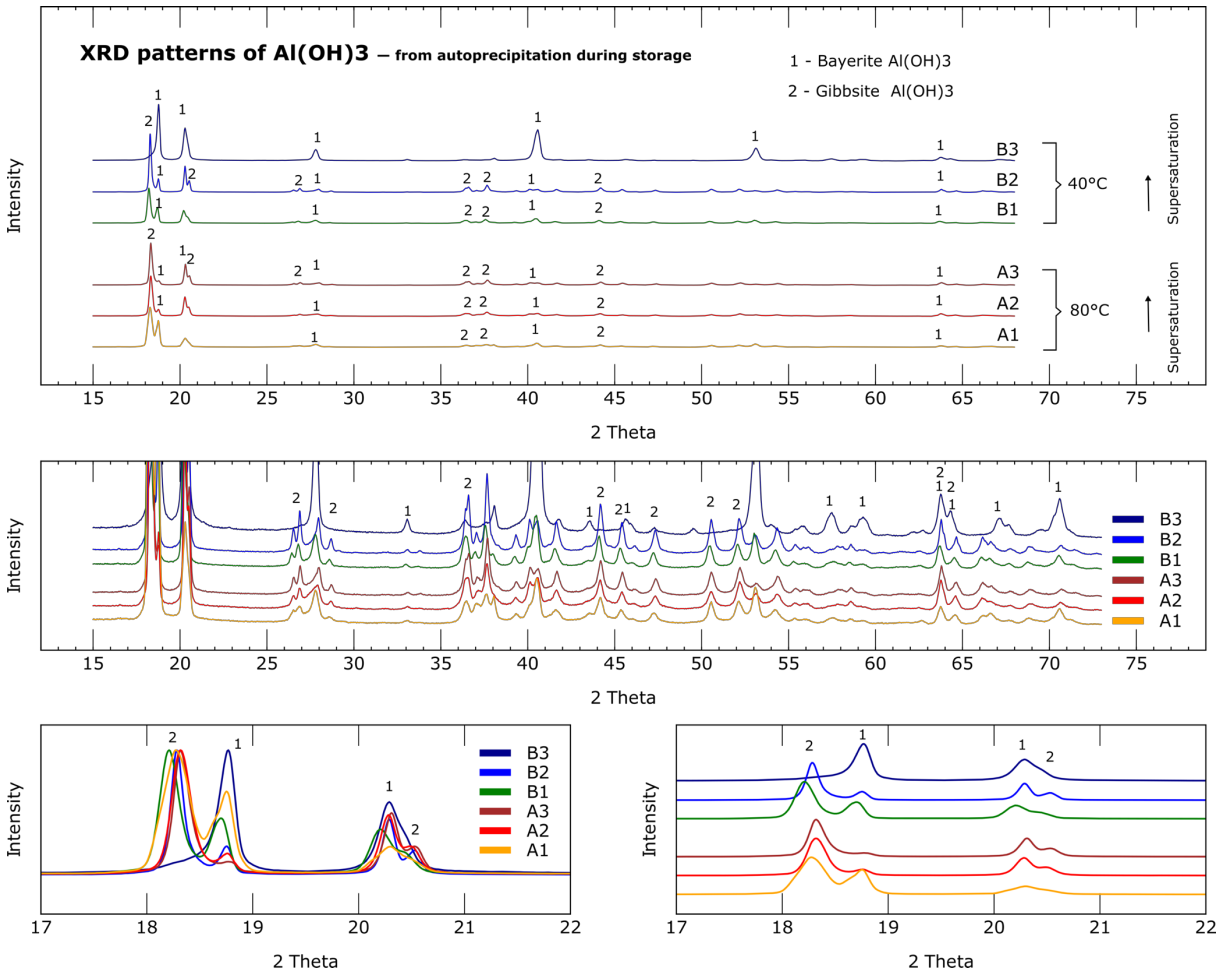

Figure 31. XRD patterns of precipitates originating from A1-3 and B1-3 experiments. The two lower patterns are normalized to the highest peak.

Precipitates from experiment C, D4 and F2 did not constitute of $Al(OH)_3$. Experiment D4 did precipitate out the AlO(OH) phase boehmite. The peaks are very broad that indicates small particles or a more amorphous structure. Dawsonite precipitate out for experiment C were carbonation lasted until pH = 9.5. The precipitate had a gel like structure and was difficult to filter out from the solution. After drying the precipitate had hard paste-like characteristics. The sodium carbonate phase natrite in combination with other $Al(OH)_3$ phases was found in the precipitate for experiment F2.

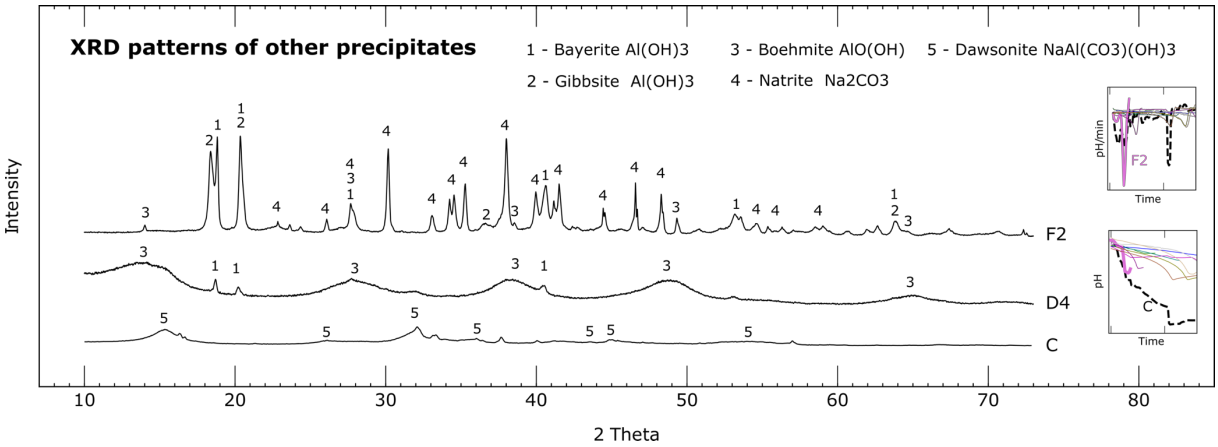

Figure 32. XRD patterns of precipitates that are not consisting of aluminium tri hydrate.

5.2.3 Particle size

The particle size distributions measured with LSD of precipitated aluminium tri hydroxides can be found in Figure 34, presented as a logarithmic distribution curves and Figure 33 presented in boxplots. The box plots make it easier to see how large most of the particles are, median size and average particle size.

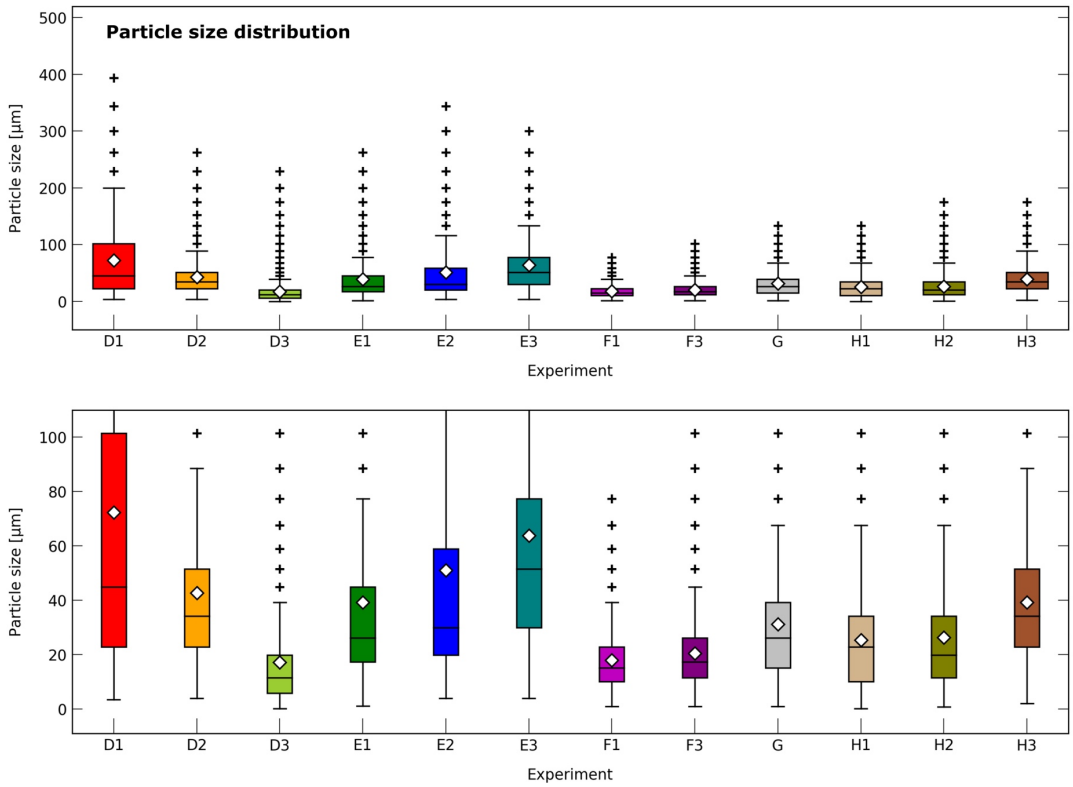

Figure 33. Particle size distribution of precipitates consisting of aluminium tri hydrate. The boxes indicate particles between 25 to 75 percentiles. The white diamond represents the mean diameter size while the line in the middle represent the media size. Crosses are outlier, particles that significantly deviates from the other particles.

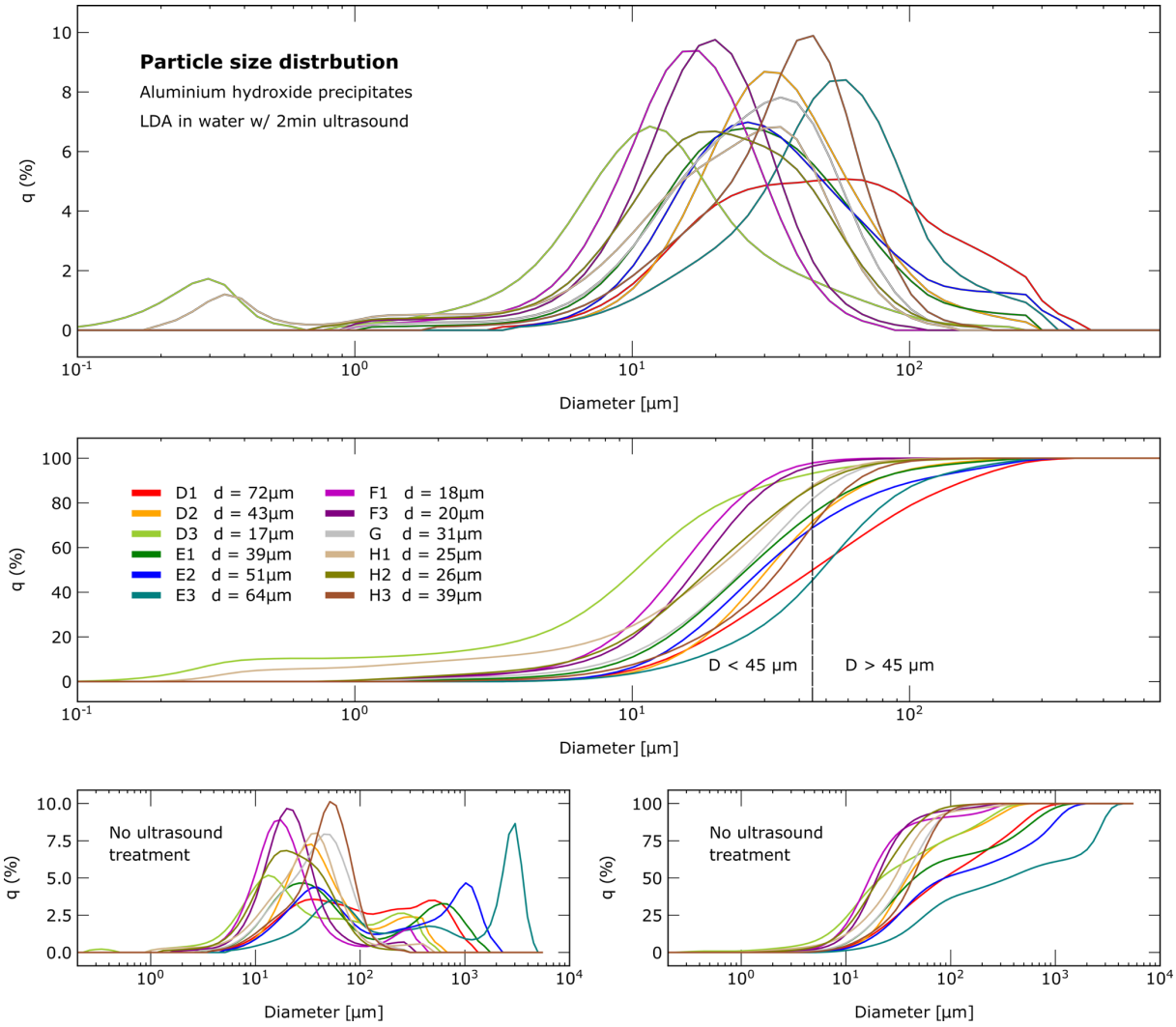

Figure 34. Particle size distribution of precipitates consisting of aluminium tri hydrate

The two lower plots in Figure 34 shows measured particle size distribution without applied ultrasound treatment to the particles to break up loose agglomerates. The average particle size of the experiments varied from 18 to 72 micrometres. Experiment H1 and D3 have small amounts of small particles in the range of 0.1-0.5 micrometre. This is the same precipitates that had most gibbsite detected in XRD analysis. The plot in the lower left corner of Figure 34 shows the particle size distribution of precipitates without used ultrasound for breaking up agglomerates. E experiments have largest proportion of large agglomerates compare to the other experiments. These agglomerates are probably very loose. Precipitates from Experiment D has the widest particle size distribution and the largest particle mean size (72um). Experiment E3 stands also out with large particle size distribution.

5.3 Chemical analysis

Chemical analysis of solution before and after precipitation are presented in Figure 35. The concentration changes and mass of precipitate per volume solution are presented in Figure 36. Almost all solutions have aluminium concentration after leaching between 19 and 24 g/L which is equivalent to 70-90 g/L Al_2O_3. The exception is experiment G were the concentration is only 40 g/L Al_2O_3. This correlates well with the amount of unreacted slag found in XRD analysis of the grey mud. After precipitation the liquors had concentration of 36-50 g/L Al_2O_3. Experiment G and H1 and the lowest concentrations after precipitation with 22 and 27 g/L Al_2O_3 which is considerable higher than 2-3 g/L Al_2O_3 that Hollum reported.

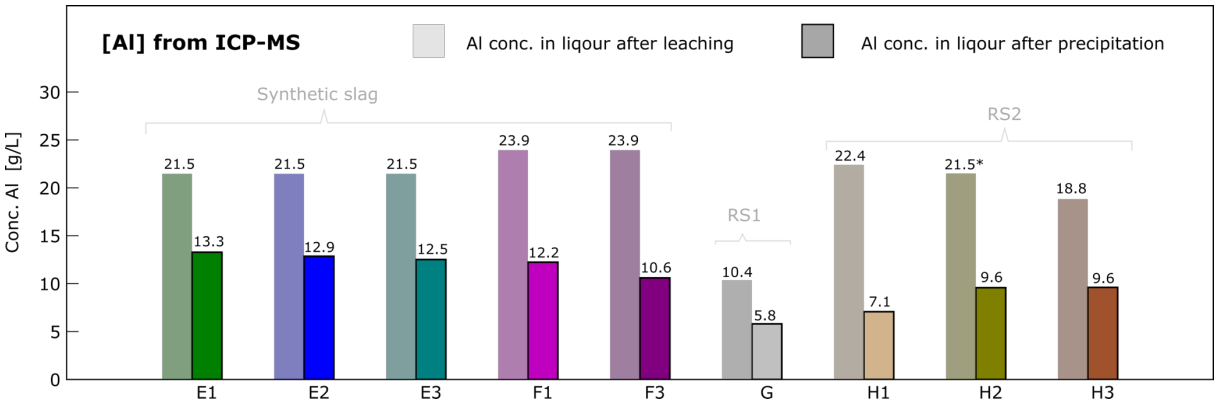

Figure 35. Chemical analysis (ICP-MS) before and after precipitation. (* estimated value)

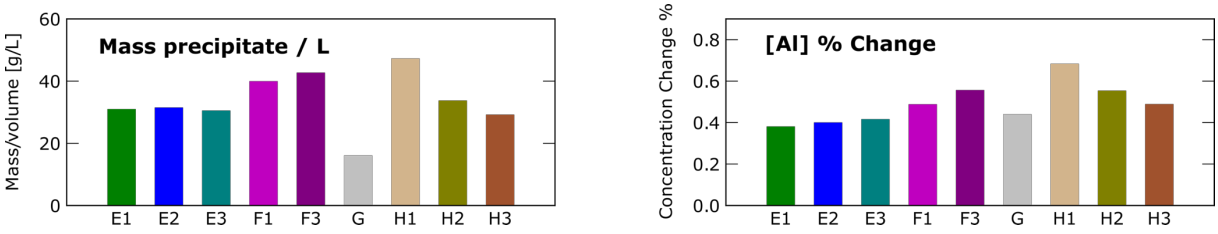

Figure 36. Mass precipitated per liter solution and percent change of alumina during precipitation.

The sodium and alumina concentration of all liquors after precipitation are presented in Figure 37. The average alumina concentration for alumina in liquors from experiment A2-3 and B1-B3 is 21.5 -+ 0.7 g/L Al_2O_3. For experiment A1 the alumina concentration is 70 g/L Al_2O_3.

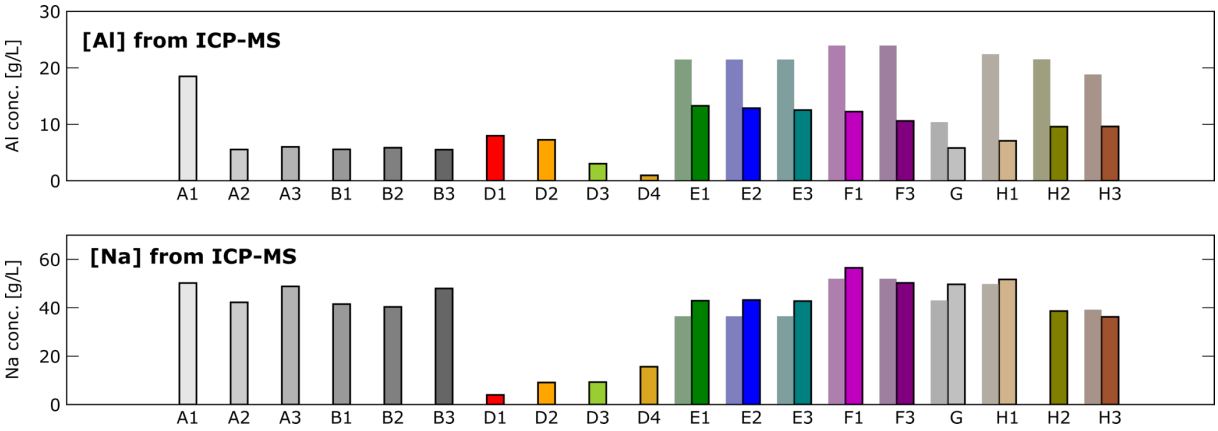

Figure 37. Chemical analysis (ICP-MS) of all samples.

In Figure 38 the pH at carbonation stop versus alumina concentration after precipitation are plotted. There is a correlation with amount carbonated e.g. pH reached and aluminium concentration. Experiments performed with low alkali concentration has a linear trend. The same is observed for high alkaline concentration. The concentration of aluminium is significantly lower at low alkaline concentration than high alkaline concentration at same pH for carbonization stop.

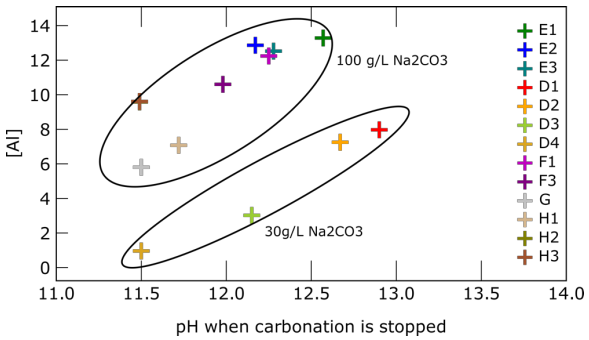

Figure 38. Aluminium concentration after precipitation versus carbonization pH stop.

The silicon concentration was analysed for experiments preformed with real slags. These are presented in Figure 39. There is unfortunately no analysis for the H2 solution after leaching. The SiO_2 concentration is calculated by comparing alumina and silica concentration. The values are ranging from 0.6 - 1.33 wt%. For the H1 experiment are the silicon concentration significantly higher in the leachate than the solution after precipitation. However, the wt% SiO_2 compared to Al_2O_3 is quite similar after leaching (1.33wt%) and for after precipitation, (1.24wt%). The silicon concentration is much lower for the H3 experiment compare to the H1 experiment. This is the opposite than expected.

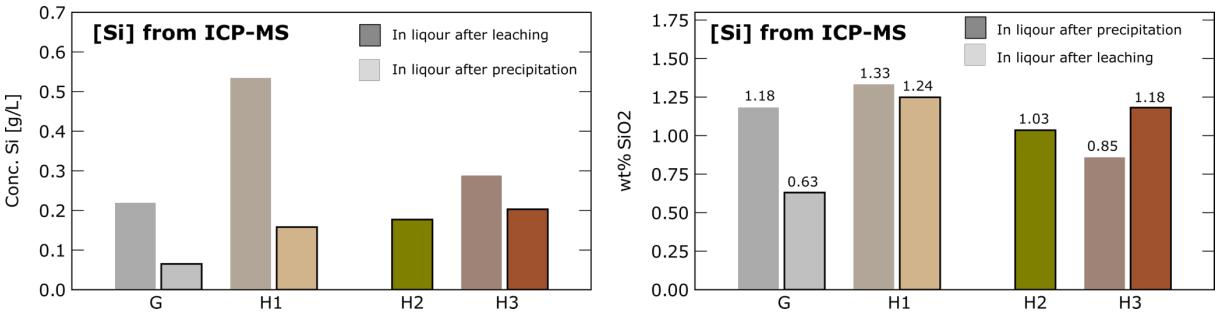

Figure 39. Silicon concentration form chemical analysis (ICP-MS) of solution before and after precipitation.

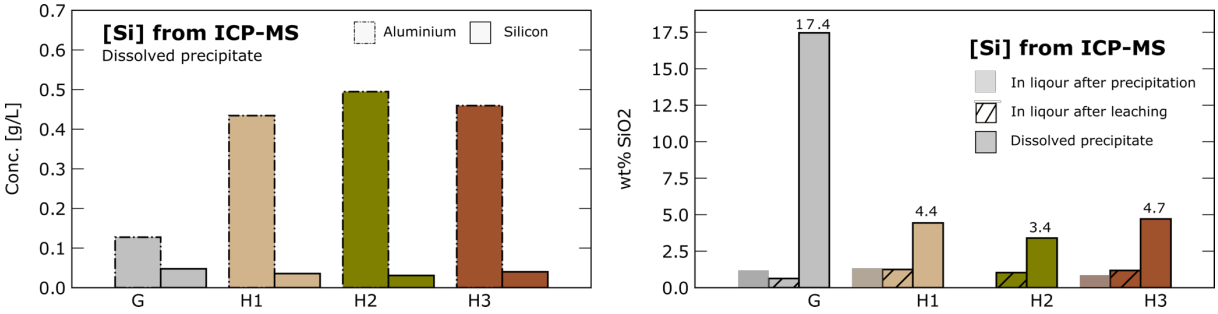

Figure 40. Chemical analysis (ICP-MS) of dissolved aluminium tri hydrate precipitates.

The silicon concentration for the dissolved aluminium hydroxide is high for the H experiments, 3.4-4.7 wt% SiO_2, and very high for the G experiment with up to 17.4 wt% SiO_2. These values are presented in Figure 40. The silica percentage is calculated from values shown in left plot in the same figure. The credibility of measured silicon concentration is discussed in Section 6.2.6.

6 Discussion

This chapter is divided into two main parts; discussion of leaching results (6.1) and discussion of precipitation results (6.2). These two main sections are divided into subsections discussing results from the different characterization or measurement methods.

6.1 Leaching

6.1.1 Grey mud characteristics – from CA based slag leaching

More unreacted slag was found in the grey mud from C12A7 based slag leaching than for the CA based slag leaching. The leaching experiments were performed with approximately the same conditions. Large parts of the CA had been hydrated to Katoite, and then reacted with $CaCO_3$ to monocarboaluminate. This may have taken place as Equation (11) and Equation (12).

$$3CA(s) + 12H_2O = Ca_3Al_2(OH)_{12}(s) + 4Al(OH)_3(s) \quad (11)$$

$$Ca_3Al_2(OH)_{12}(s) + CaCO_3(s) + 5H_2O(l) = Ca_4Al_2(CO_3)(OH)_{12}(H_2O)_5(s) \quad (12)$$

Reaction (11) has a low free energy (ΔG = -27 kJ/mol) and is highly exotherm (ΔH = -215 kJ/mol). Reaction (12) is shifted more to the right at lower temperatures as ΔG is equal 8.5 kJ/mol at 25°C and 12kJ/mol at 90°C. This indicates that monocarboaluminate is more stable at lower temperatures. This is consistent with what seen in XRD patterns (Figure 20). At lower temperatures only monocarboaluminate and no Katoite is found in the XRD patterns, but at higher temperatures peaks representing Katoite and monocarboaluminate share the same intensity. Reaction (12) has a positive free energy for an ideal system, but the system studied is not ideal and might be negative for experimental condition. The reaction mechanism might also be different than the proposed reaction 12.

More Nordstrandite compare to Bayerite has been found in in grey mud from experiments with higher slag to liquid ratios and higher leaching temperatures. The grey mud from experiment B2 had significantly more Nordstrandite than in the grey mud from experiment B1 and B3. The

grey mud was also the only grey mud of the three that had Katoite. Nordstrandite might therefore be related to Katoite formation. Azof *et al.* (2019) also found $Al(OH)_3$ in presence with Katoite. They used lower solid to liquid ratio and Bayerite was the only aluminium hydroxide phase observed. Therefore, the initial $Al(OH)_3$ precipitation may take the form of Bayerite, but as the chemical conditions changes during leaching with high solid to liquid ratio Nordstrandite forms.

6.1.2 Grey mud characteristics – from C3A and C12A7 based slag leaching

C12A7 does not hydrate like CA. No monocarboaluminate and very little Katoite is found in the grey mud from experiment with the C12A7 based slag. The small amount of Katoite originates from the small amount of CA in the slag. Similar observation can be seen in (Azof *et al.*, 2019) where Katoite is found in grey mud originating from CA based slags.

An unidentified phase was found in the XRD pattern of the grey mud originated from the H1 experiment, the experiment with highest leaching temperature of the C12A7 based slag. The $CaCO_3$ amount was significantly lower in this grey mud compare to grey mud from the H2 and the H3 experiment. This indicates that the unidentified phase is a product of a reaction where $CaCO_3$ is a reactant. There is not significantly lower concentration of C12A7 in the grey mud where the phase appears. The phase might therefore have formed from species in the solution. The author guesses the phase is a calcium carboaluminate or another type of a hydro garnet.

The other unidentified peaks in the grey muds had some correlation with reference peaks in the PDF database but the author found it difficult to claim that these peaks could be correctly identified. The unidentified peak at two theta equal 31.0 might be the phase Gonnardite, $(Na,Ca)_2(Si,Al)_5O10.3H_2O$. The unidentified peak at two theta equal 11.8 might be the calcium carboaluminate, $Ca_4Al_2O_6CO_3.11H_2O$. The peak resembles monocarboaluminate that was found at low temperatures and similar slag to solid ratio, but with different slag composition. The phase Trebeurdenite, $Fe(CO_3)_{0.17}(OH)_2(H_2O)_{0.5}$ has also good match with the peak at two theta equal 11.8.

6.1.3 Alumina extraction

The slag composition is important for the alumina extraction during leaching. The solution originated from leaching of the C3A based slag (RS1) had much lower alumina concentration

(40 g/L) than the solution originated from the C12A7 based slag (RS2) and the synthetic slag (70-90 g/L). Unfortunately, many of the chemical analysis of the solutions originating from the CA based slag were ruined. The degree of supersaturation as function of solid to liquid ratio could not be determined for A and B experiments. However, the solutions seemed highly supersaturated considering the amount of $Al(OH)_3$ precipitating during storage. The solutions from high solid to liquid ration seemed the most supersaturated. The large amount of water absorbed when hydrates are formed during leaching affect the degree of supersaturation. This is more pronounced for experiments with higher solid to liquid ratios. The absorption minimizes the solution volume and therefore increase the alumina concentration. This is an important aspect when designing a process using high solid to liquid ratios. Especially if the process is based on a slag that can easily hydrate.

Mure Hollum *et al.*, (1951) used an even higher solid to liquid ratio compare to the experiments in this study. They got approximately the same alumina concentrations for the saturated solution as in the E, F and H experiments. Around 80-90 g/L alumina may be an upper saturation limit for leaching with high solid to liquid ratios and with alkali concentration around 100 g/L Na_2CO_3. More experiments with different slags at high solid to liquid ratio must be executed to confirm this.

The grey mud originated from the synthetic CA based slag had significant amount of solid aluminium hydroxide. A more alkaline solution with the addition of free NaOH should dissolve the aluminium hydroxide and increase the aluminium yield. This would not be the same case for the C12A7 based slag where solid aluminium hydroxide does not exist. The extraction rate is limited by dissolved Na_2CO_3 reacting directly with C12A7. An industrial process using a CA based slag would most probably not get the benefits of a self-disintegrating process because C2AS will form instead of the C2S phase that stands for the self-disintegrating phenomena. In the other hand lower lime consumption is needed to form CA, and the aluminium yield might be better when using leaching conditions adapted for a highly productive process.

Only $CaCO_3$ and unreacted C3A slag were observed in the grey mud of experiment G. The solution leaching in the experiment had much lower aluminium concentration than experiments with the CA and C12A7 based slags. The leachability of the studied slags correlates well with the literature and confirming that C12A7 and CA are highly leachable phases compare to C3A.

6.1.4 Silica impurities in leachate

The silicon concentration was not lower for H1 performed at 90°C than H3 performed at 50°C. This stands in contradiction to experimental results presented by Mure Hollum *et al.*, (1951). The solutions from the H experiments had concentrations around 1wt% SiO_2 compare to Al_2O_3 concentration. This silica concentration is too high for precipitating out high quality metallurgical aluminium hydroxide. High quality alumina has under 0.02wt% SiO_2. The concentrations of SiO_2 in solutions H1 and H3 after leaching were 1.14 g/L SiO_2 and 0.616 g/L SiO_2, and the solutions presented by Hollum had SiO_2 concentrations lower than 0.02 g/L. The alumina concentration of the solutions was approximately the same in Hollums paper as in this study. Some experimental conditions were different compare to Hollums patent; no free NaOH was added as part of total alkali concentration, Hollum used a larger solid to liquid ratio and the composition of the slag used by Hollum is unknown. The addition of free NaOH might dissolved $Al(OH)_3$ found in the CA based slag. This would increase the alumina concentration of the solution and decrease the SiO_2/Al_2O_3 ratio in the liquor.

The silica solubility cannot instantly decrease at a certain temperature. Other mechanisms of silica reduction must be related to what Mure Hollum *et al.*, (1951) reported. The author expected that the grey mud would change composition at higher temperature, bind silica and reduce the silica concentration in the leachate. The silicon containing phase might not be leachable in a second leaching step. A new phase in the grey mud was observed for the high temperature experiment H1, but the silicon concentration was not lower. However, too few experiments are conducted to falsify the author's theory and more experiments are needed to investigate the correlation of grey mud composition and silicon concentration.

6.1.5 Possible synergies between grey mud and silica concentration in leachate

The silica distribution between leachate and grey mud for CA slag leaching may be different from C12A7 slag leaching because the hydration of CA. The silica concentration was not analysed for solutions obtained by CA slag leaching. The synthetic CA slag was low in silica and aspects related to silica impurities were not emphasised during the preliminary experiments. However, studying CA based slag with higher silicon content would be interesting. Silicon may be bound to different phases in the grey mud and leaving a purer solution for precipitation. More research should be performed exploring synergies between grey mud composition and silica concentration in leaching solutions. Different solid liquid ratio, temperature and slag

composition could give different beneficial grey mud compositions. The leachabilities of a second leaching step of the grey mud should also be studied. This is important for the alumina yield of the process when using high solid to liquid ratios. A process with low alumina yield will not be economical sustainable.

6.1.6 Consequences of silica impurities for a high alkaline Pedersen process route

A process using Na_2CO_3 for leaching and carbonation for precipitation can most likely not be used without a desilication process. As mention before, desilication processes are used for nepheline processing and for the sinter method. This must most likely also be implemented to a Pedersen process that uses high alkaline concentrations. The low concentration variation, which was used at the Høyanger plant, can also be used. But this variation does not get the benefits of high productivity and a low tank volume. The desilication process involves the addition of $Ca(OH)_2$ to the solution. Large amount of lime used for the smelting (to obtain a disintegrating slag) and the amount for desilication step might be the largest challenge for such a process.

6.1.7 Possible processes for low-silica alumina

Developing new process concepts for reducing the silicon impurities without adding new lime to the system require more research. A process with high alumina yield, low silica impurities without adding new reactants to the system will be beneficial for an economical sustainable process. Ideas can be gathered from the calcification-carbonation method (Zhang *et al.*, 2016) to create a process that exploits the hydro garnet formation in the grey mud when leaching with high solid to liquid ratios. This process shows that hydro garnets can decomposed to $Al(OH)_3$, Ca_2SiO_4 and $CaCO_3$ by carbonation. The alumina can then be selectively leached with a NaOH solution from the decomposition products, and by this separating SiO_2 and Al_2O_3 compounds.

6.1.8 Leaching mechanism proceeding

Measuring temperature and pH simultaneously during leaching gives helpful information for understanding what reactions taking place during leaching. The hydroxide ion is one of the most important reactants (or products) for reactions in aquatic solutions and the temperature changes indicate if reactions are endothermic or exothermic. Figure 41 shows a generalized sketch of how hydroxide and temperature curves look like for the leaching experiments. The

sketch helps assessing when reactions occur, and the author has divided the curves into five distinctive sections that have specific characteristics.

Calcium aluminates, calcium aluminate hydrates and calcium carbo aluminates are found in the grey muds. These phases are also studied within cement chemistry. Thermal analysis of cements formation how different phases form can be found in literature (De Weerdt, 2007). This can be helpful for understanding grey mud formation during leaching.

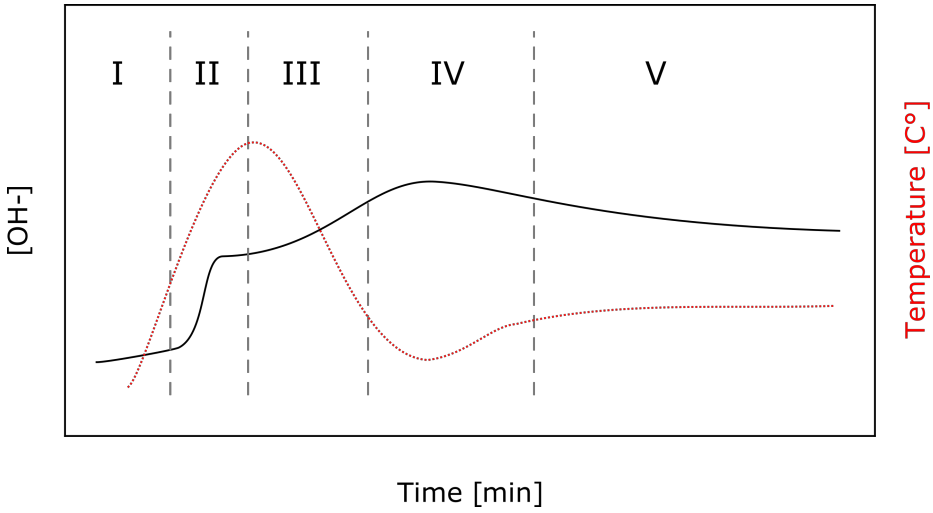

Figure 41. Qualitative sketch of hydroxide concentration and temperatures changes versus time during leaching. The section is divided into five steps that may be representative for different reaction mechanisms or sections where certain reactions dominates.

I. A slow temperature increase for low temperature experiments with the synthetic slag are observed. This is probably only heat supplied from hot-plate and not originated from chemical reaction. The experiments done at high temperatures or experiments with the real slags has a very short step I or starts directly on step II. This indicate that step two has an activation barrier that is temperature dependent.

II. Step two is characterized by rapid increase of pH and temperature. The pH increase is much prominent for low temperature experiments. The pH increase suddenly levels out after short time and for some experiment decrees slightly. The temperature increase stops when the step two is over. This step may be associated with dissolution of different species and rapid reactions taking place on particle surfaces. Hydration reactions are often very exothermic and large parts of the temperature increase can originate from

this. Reaction (11) has an ΔH = -215 kJ/mol and large fraction of this Katoite and $Al(OH)_3$ is already found after 10 min of leaching by Azof *et al.* (2019). This indicates that hydration reaction take place early during leaching for CA based slags.

III. Temperature is decreasing rapidly, and pH increase steadily. Polymerization reaction are often endothermic. The carbonate ions react with calcium atoms in the slag breaking up the slag structure. The increase of pH can be influenced of the decrease of temperature that increases pH. It is also reported that the formation of calcium carboaluminates are strongly endothermic when occurring in cements (De Weerdt, 2007). The decrease of temperature may originate from the formation of calcium aluminate hydrates to calcium carboaluminates.

IV. Endothermic reaction stops. Heat supplied from the hot plate increases the temperature. It might also be exothermic reactions that increasing the temperature, but the author thinks most of the temperature increase comes from the hot-plate.

V. A stable pH and temperature are observed. The leaching reaction may be over or significantly slower.

The leaching set-up is an open system. Heat are lost and supplied to the system and there are many sources of error. The set-up is not ideal for thermal analysis. Some precipitation of $CaCO_3$ were also observed of the pH electrode after leaching. This may also affect the pH and temperature curves. Especially during the preliminary experiments, the author had feeling that the pH meter operated somewhat peculiar. Conclusion on mechanisms proceedings drawn from measurement curves are somewhat speculative.

6.2 Precipitation

6.2.1 Reactions occurrence based on pH and temperature measurements

Absorption of CO_2 results in consumption of hydroxide ions. The pH measurement plot illustrates this clearly. The OH^- concentration rate change decrease slightly with time. This is a result of aluminium hydroxide precipitation (which produce OH^-) and less OH^- that can react with CO_2 gas. The absorption of CO_2 gas is very exothermic (ΔH = -109 kJ mol^{-1}) and therefore solution temperature increases by carbonation. The temperature increases rapidly when

carbonation starts but declines (and later decreases) when endothermic processes starts to dominate. The temperature decreases even though the CO_2 absorption rate is high. This can be seen in the pH plots as OH^- concentration steadily declines simultaneously as temperature. Depolymerization of $Al(OH)4^-$ is slightly exothermic (ΔH = -36.8 kJ mol^{-1}) and the temperature decrease cannot come from the bulk chemical energy change. The temperature decrease comes from the creation of interfaces between aluminium hydroxide and the solution. As the nucleates are nanosized, energies related to the interfacial area can be more significant than the bulk energy. The interfacial energy between the precipitates and the solution is high. This energy has to be supplied to the system to create interfaces. This energy is heat, and the creation of the interfaces is therefore endothermic. The fact that the temperature decreases after the purging stops, exclude theories that the gas cools the liquid. The thermodynamic data for polymerization of hydroxide aluminate ions might also be wrong. It might be endothermic for the system studied.

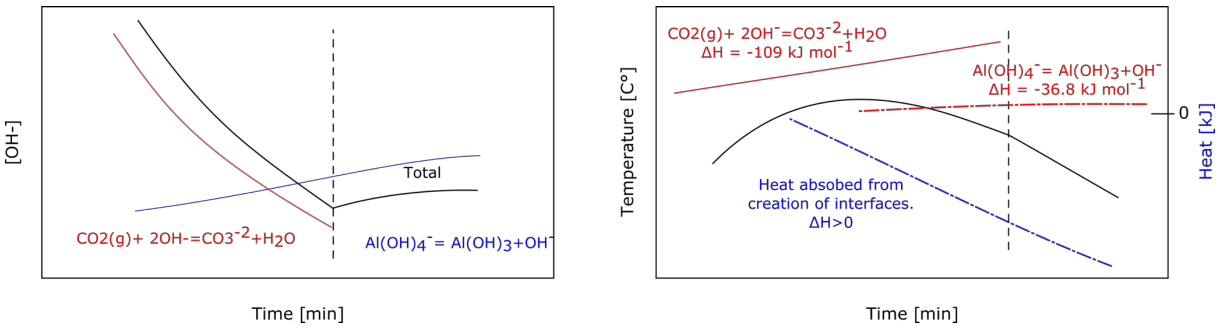

Figure 42. Qualitative sketch of typical pH (left) and temperature (right) curve for carbonization experiments performed. The heat curves in the right figure represent total accumulated heat for each phenomenon.

For experiment F3 (were high CO_2 partial pressure and flow were used) the exothermic CO_2 absorption is much larger than the precipitation of aluminium hydroxide resulting in increasing temperature until the purging stops. Then the temperature drops immediately by endothermic interface creations.

With in-situ pH and temperate measurement, the aluminium hydroxide precipitation rate could be determined in-situ. The rate of OH^- is a function of CO_2 absorption and $Al(OH)_4^-$ decomposition. This could be modelled and with the help the rate of OH^- decrease could determine the aluminium hydroxide precipitation rate during carbonation and even simpler

when carbonation stops from the increase of OH^- concentration. This could be beneficial for operating an industrial process.

6.2.2 Gas-liquid interface

High CO_2 gas flow rates and large CO_2 partial pressure result in decreased OH^- concentration and increased CO_3^{2-} concentration near bubble interfaces. The solubility of $Al(OH)_4^-$ will therefore be lower near interfaces and nucleation will first appear close to bubble interfaces. This was clearly seen from nucleation clusters coming down from bubbles bursting between then solution-atmosphere interface from experiment G and H1-3. Gas bubbles attached to liquid interface had a longer retention time allowing more CO_2 absorbing into the solution and creating local low concentration of OH^-. A higher CO_2 partial pressure gives higher local concentration difference at the interface compare to bulk concentration. A high partial pressure should be avoided when using high concentration solution and large gas flows. The gas mix can be too aggressive and result in unwanted phases or uncontrolled nucleation. The precipitation from solution-atmosphere interface was evident for experiments with $Pco_2 = 0.33$ and gas flow equal 1.5 $slpm^{-1}$ (standard liter per minute). The partial pressure should be lower than this for avoiding unwanted interfacial effects.

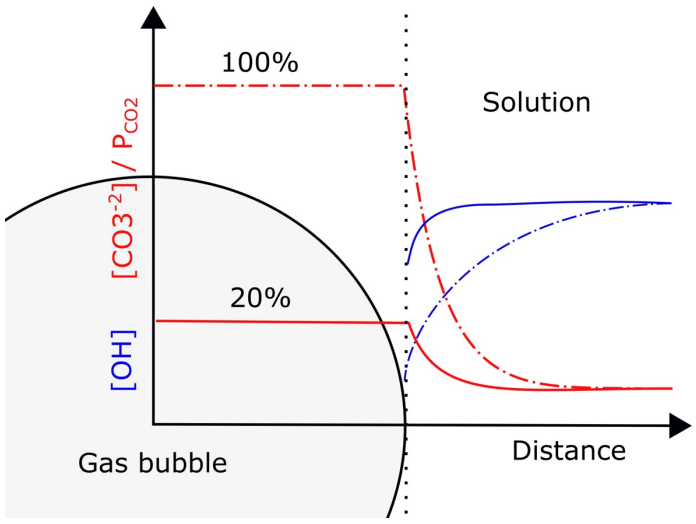

Figure 43. Illustrative sketch of concentration profiles of reactants near a bubble-solution interfaces for high and low CO_2 partial pressure.

When the gas flow meter failed on experiment F2 100% CO_2 flowed into the solution with high flow rate. The concentration of CO_3^{2-} and HCO_3^- became so high at the bubble solution interface that it reacted with Na to form solid Na_2CO_3.

6.2.3 Precipitate characteristics

There is no problem to precipitate out $Al(OH)_3$ from highly concentrated sodium aluminate solutions by carbonation. Out of 15 experiment, 13 precipitation resulted in $Al(OH)_3$, one in AlO(OH), one on Na_2CO_3 and one with Dawsonite. For the C experiment the amount of CO_2 absorbed resulted in the formation of Dawsonite. The system had clearly reached section 3 in Figure 7, either at the interfaces or for the bulk solution.

The carbonation rate is an important factor for the phase composition of the precipitates. The absorption rate of CO_2 (g) is faster than the depolymerization of $Al(OH)_4^-$. This can clearly be seen from the pH logging curves. The driving force for CO_2(g) absorption kinetics (ΔG = -56 kJ/mol for reaction (3)) is also larger than the driving force for depolymerization reaction kinetics (ΔG = -10.5 kJ/mol for reaction (2)) and a higher driving force often results in faster reactions. The carbonation rate determine the OH^- / $Al(OH)_4^-$ concentration ratio which determine the aluminium hydroxide phase precipitated (Czajkowski, Noworyta and Krotki, 1981).

At a high nucleation rate, OH^- hydroxides are produced at a high rate. This was observed during experiment H1 as the pH stopped decreasing during carbonation and levelled out. When carbonation was stopped right after the out levelling and the high degree of nucleation can be observed from the pH measurement curves (see Figure 26). The curve is more rounded compare to other measurements during carbonation stops, and the pH rate is significantly larger than the other measurements after the carbonation stops. There was a high degree of homogenous nucleation. This led to precipitation of gibbsite as the OH- / $Al(OH)_4^-$ decreased as a result of OH- production. The XRD peak for gibbsite is significantly larger for experiment H1 and D3. There was no pH measurement of experiment D3, but the carbonation stopped at relatively low pH giving a high degree of supersaturation. The CO_2 partial pressure was equal 1 and larger parts of the precipitation has most likely been precipitated from the gas-liquid interface. The carbonation was stopped at an even lower pH for D4 than D3. This resulted in boehmite precipitation, most likely originated from the gas-liquid interface. The OH^- formation from depolymerization of $Al(OH)_4^-$ pushed the system into $OH^-/Al(OH)_4^-$ ratio region where boehmite is formed. The sodium concentration was low for this experiment. This might have reduced the possibility to form sodium-based phases as dawsonite.

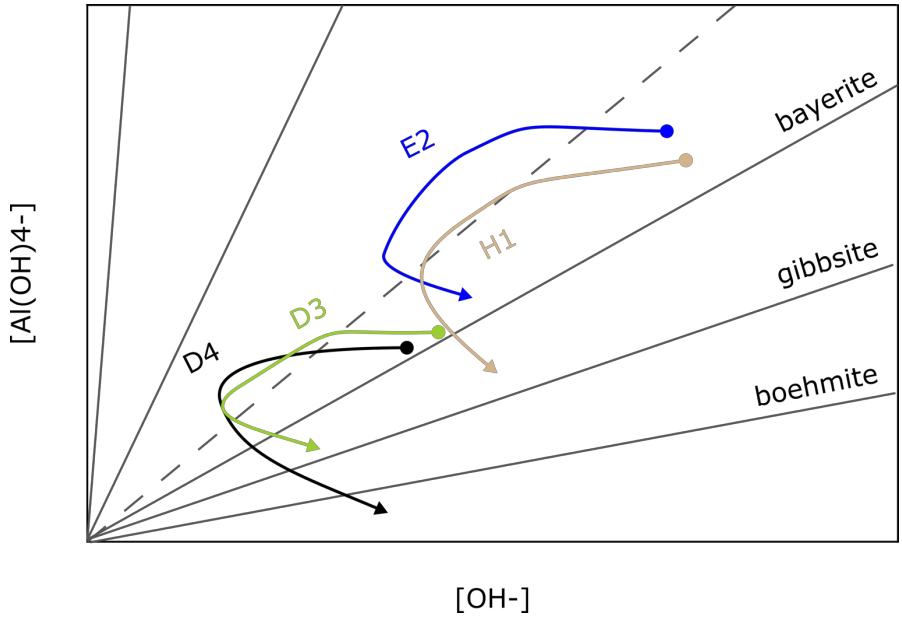

Figure 44. Phase equillibrium in aluminate solution – $Al(OH)_3$ as function of ion fraction. Possible curves of how concentration D3, D4, H1 and E2 occurs has been drawn into plot. The plot is redrawn from *Czajkowski, Noworyta and Krotki, (1981)*.

The theory of phase precipitated determined from the $OH/Al(OH)_4^-$ ratio is based on the paper (Czajkowski, Noworyta and Krotki, 1981). They are citing other papers claiming this relationship, but these papers could not be found. Figure 44 is a plot redrawn from the paper. Equilibrium lines of aluminium hydroxide polymorphs are presented in a $[OH^-]$ versus $[Al(OH)_4^-]$ plot. Qualitative interpretations, based on XRD analysis and pH measurements, of how ion concentration changed during carbonations for selected experiments are drawn into the figure. The curves start first with reduction OH^- concentration as result of carbonation. No polymerization of aluminate ions occurs. When the polymerization of aluminate ions starts, hydroxide ions are produced at the same time as other hydroxide ions are consumed by carbonation. The degree of precipitation versus carbonation determine the hydroxide ion concentration change. When carbonation stops OH- are produced and $Al(OH)_4^-$ continue to decompose.

6.2.4 Auto precipitates

B3 deviates from other by forming only Bayerite. This solution has might been the most supersaturated. A higher $Al(OH)_4^-$ should push the system into the Bayerite formation area. By the appearance of the precipitate A3 and B3 looked like $Al(OH)_3$ had been homogenously or

heterogeneously precipitated. The $Al(OH)_3$ from the other samples looked like crystal growth had happened on the container wall. The author found it hard to explain why the different phases appeared, but the crystallisation type (growth or heterogenous nucleation) might affect what phase precipitates.

6.2.5 Precipitation yield

Around 50% of the alumina was precipitated for the experiments and the solutions of had a concentration between 22 and 50 g/L Al_2O_3. The solution should have been carbonized further to obtain a better yield. The Hollum patent had a concentration down to 2 g/L Al_2O_3 after carbonisation. More work should be carried out determining the carbonation duration for reaching maximum yield. In retrospect carbonization experiment studying aluminium yield by vary carbonation time should have been executed as this is a key feature for precipitation from carbonization. As many chemical analyses were damaged early in the work process, the yield could not be determined before the last experiments. This made it difficult to make the decision of designing experiments for study alumina yield.

6.2.6 Silica impurities in precipitates

Silica is more unstable than aluminium hydroxide in sodium aluminate solutions. All the silica precipitates during the start of carbonation. A low alumina yield will therefore give a high silica content in the precipitate. The silicon concentration measured from dissolved aluminium hydroxides was high. The silica concentration for experiment H1, H2, and H3 were equal 4.4, 3.4 and 4.7 wt%. Aluminium hydroxides obtained from H1-3 have too high silica concentration for further processing to smelter grade alumina.

Aluminium hydroxide from the G experiment had a silicon concentration of 17wt%, but the XRD pattern of same precipitate indicated 100% aluminium hydroxide. The author believes that solubility of silicon in solid aluminium hydroxide cannot be that high. The silicon should form new phases. The analysis results be trusted and should been repeated. The precipitates could have been dissolved in different solutions (acids and bases) to validate the concentration measurements with ICP-MS. The concentration could also be checked with XRF analysis, but author had insufficient time to perform such analysis (due to inaccessible lab facilities).

First off all is a cleaner solution after leaching needed for obtaining aluminium hydroxide with acceptable concentration of silica. However, long carbonation times (10h) at higher temperatures (around 80°C) resulted in less silica for carbonation experiments related to the syenite nepheline process (Shayanfar *et al.,* 2018). Carbonisation conditions for achieving aluinium hydroxide low in silica should be studied. This is essential for devoloping new processes without a desilication step.

6.2.7 Particle size

Most of particles precipitated cannot be qualified as high quality due to a low particle size. The best obtained results were for experiment D1 and E3. Approximately half of these particles are larger than 45µm, which is the minimum desired particle size. Understanding the mechanism behind the best obtained result can help further research for optimizing product particle size.

Stirring rate was not carefully enough noted and controlled during the precipitation experiments. This is an important factor for agglomeration and particle growth. The D experiments were performed with very low stirring rate. The D1 experiment, with lowest supersaturation (and presumably the lowest precipitation rates), obtained the largest particle size distribution. High stirring rates were used for the E experiments. Here the experiment with highest supersaturation, E3, got the largest particle size distribution. There might be correlation between nucleation rate and stirring rate that gives highest degree of agglomeration. At low stirring rate a low nucleation rate could give high degree of agglomeration and at high stirring rates a high nucleation rate could give high degree of agglomeration. Scanning electron microscopy images of particles could help determine if the particles are mainly agglomerated or grown together. The author did not have sufficient time executing such characterization.

The precipitates with larger amounts of Gibbsite (from the D3 and H1 experiment) had a small fraction of nanosized particles (>1µm) that was not observed in other experiments. The particles stand for approximately 10% of the total numbers of particles. As discussed earlier, the Gibbsite formation is a result of fast rate and fast production of OH^-. The fast and homogenous nucleation occurring during carbonation stop resulted in portions of small particle size that did not further agglomerate. This is what seen in the particle size distribution analysis.

6.2.8 Carbonation control

In this study carbonation was stopped when the solution reached a certain pH because this was also used at the Høyanger plant to determine the degree of carbonation. At high nucleation rates, the net change of OH^- can be positive resulting in pH increase. At the end of carbonation in experiment H1, OH^- production was almost as large as OH^- consumption and further carbonation would result in pH increase. Studying how the curve would turn out with further carbonation could be of interest for understanding the precipitation rates as function of time. The author would not carbonate the solutions to lower pH equal 11.5 for the experiments due to the uncertainty of formation of unwanted phases. As mention before, longer carbonation duration should be applied to lower the alumina solubility for achieving a better yield. The author thinks that performing further carbonation experiments should be done with low CO_2 pressure, varying the total gas flow and stop carbonation as function of time (not pH). Carbonation is often studied for constant flows. A different carbonation program with stepwise purging could maybe lead to preferable nucleation for increased particle size.

7 Conclusion

The main findings of this thesis concern experimental set-up and procedures for leaching and precipitation by carbonation, precipitate and grey mud characteristics and silica impurity challenges. Executing experiments for exploring new systems can lead to many errors. Some practical issues learned from experiments performed are listed below. These are important to avoid when designing leaching and carbonization experiments. This can facilitate faster progress for later research.

- Samples taken after leaching for ICP-MS analysis must be mixed with highly alkaline solutions to avoid auto precipitation during intermediate storage.
- Purging stones with small pore dimensions is not suitable for use in carbonization experiments as they are clogging by precipitates.
- Chemical analysis of aluminium hydroxides should be backed up with other analysing techniques than ICP-MS of dissolved precipitates in sodium hydroxide. This could be XRF or ICP-MS of another solvent used.

Important information can be gathered from pH and temperature measurement during leaching and carbonization. The carbonization and precipitation rate can be found from pH curves and the reaction activity can be interpreted from temperature curves of leaching. The author suggest that the length of carbonization experiments should be decided by time and not by reaching a specific pH value.

Many important features for precipitation by carbonization have been discovered from the experiments performed. Some of the key features are listed below.

- Aluminium hydroxide can easily be precipitated from highly alkaline sodium aluminate solutions.
- Lower carbon dioxide partial pressure avoids interfacial effects that can result in unexpected phase formation from local concentration differences. These interfacial effects can also make it difficult to controlling particle size distribution.
- The aluminium tri hydroxide polymorph formed during carbonization is dependent on the hydroxide ion / aluminate ion fraction. The fraction can be different at the

bubble solution interface. The quantitative ion fraction resulting in different polymorph could not be determined, but qualitive information correlates good with literature.

- Silicon compounds precipitate first during carbonization. It is important to get a high alumina yield for obtaining less as possible silicon contamination in the final precipitate. The solutions obtained after leaching needed a higher degree of carbonization to achieve higher yield.

The agitation speed during precipitation experiments was not sufficiently documented for determining which conditions enhance agglomeration and particle growth. Though, the particle size distribution for some experiments indicates that a preferable particles size distribution can be obtained for precipitates originated from a carbonization process.

The leaching results obtained were limited due to lack of chemical analysis. However, several interesting findings related to grey mud are listed below.

- The CA based slag hydrolysed much faster than the C12A7 based slag. The CA hydrolysis product Katoite is more pronounced at higher temperatures and larger solid to liquid ratios.
- Calcium carbonates are less pronounced at higher solid to liquid ratios.
- The occurrence of the aluminium hydroxide polymorph Nordstrandite may be related to formation of Katoite.
- Monocarboaluminate is more stable at low temperatures for CA based slag.
- An unidentified phase found in XRD pattern for C12A7 based slag needs to be characterized.

This Thesis confirms that CA and C12A7 based slags are highly leachable in sodium carbonate solutions (considerably more leachable than C3A based slags). However, they behave differently when leached with high solid to liquid ratios. This can be beneficial for different variations of the Pedersen process. The CA formation needs less lime for bauxite smelting. It has interesting characteristics for leaching with high alkaline concentrations. The phase hydrolyses and creates solid aluminium hydroxide in the grey mud. This can be dissolved in higher alkaline concentration, either in the first leaching step (with addition of free NaOH) or

in a second leaching step. The hydrolysed slag might be beneficial for a high alumina yield when leaching in several steps. In the other hand CA based slags does not self-disintegrate after smelting because silicon will be bound to the C2SA phase and not to C2S that cause the disintegration. A C12A7 based slag will most probably be self-disintegrated but do not change character as much CA during leaching. The performance of a second leaching step should be studied for both slags at high solid to liquid ratio.

The silicon impurity concentration was too high for experiments performed with a C12A7 based slag at high temperature and high alkali concentration. A desilication process step most be integrated in a conventional Pedersen process using high alkaline concentrations. Alternatively can new process concepts be developed. Ideas of how silicon can be bound to the grey mud should therefore be studied. The formation of complex hydrates can possibly bind silicon and hinder high concentration of silicon in the leachate. These phases can might be decomposed into calcium silicates in a second decomposition treatment and separate the silicon from aluminium in solution.

The Thesis concludes with pointing out knowledge gaps that need to be filled for operating a sustainable Pedersen process. The performance of a second leaching step must be examined to improve the yield of the process if intermediate to large solid to liquid ratios are used. How to control the carbonation for optimizing yield and particle size distribution is important for exploiting the advantages of precipitation by carbonization. This Thesis forms a basis for further research on leaching and carbonization related to the Pedersen process that might lead to a sustainable and more environmentally friendly alumina production.

8 References

Aleva, G. J. . (1994) *Laterites. Concepts, geology, morphology and chemistry.* ISRIC, Wagningen.

Azof, F. I. *et al.* (2019) 'Leaching characteristics and mechanism of the synthetic calcium-aluminate slags for alumina recovery', *Hydrometallurgy*. Elsevier, 185(November 2018), pp. 273–290.

Azof, F. I., Kolbeinsen, L. and Safarian, J. (2017) 'The Leachability of Calcium Aluminate Phases in Slags for the Extraction of Alumina', *Proceedings of 35th International ICSOBA Conference*.

Azof, F. I., Kolbeinsen, L. and Safarian, J. (2018) 'Characteristics of Calcium-Aluminate Slags and Pig Iron Produced from Smelting-Reduction of Low-Grade Bauxites', *Metallurgical and Materials Transactions B*. Springer US.

Bai, G. H. *et al.* (2010) 'Alkali desilicated coal fly ash as substitute of bauxite in lime-soda sintering process for aluminum production', *Transactions of Nonferrous Metals Society of China (English Edition)*. The Nonferrous Metals Society of China, 20, pp. s169–s175.

Blake, H. E. *et al.* (1966) 'Adaption of The Pedersen Process to The Ferruginous Bauxites of Pacific Northwest', *INT.-BU OF MINES, PGH.,PA.*

Czajkowski, A., Noworyta, A. and Krotki, M. (1981) 'Studies and modelling of the process of decomposition of aluminate solution by carbonation', *Hydrometallurgy*, 7, pp. 253–261.

Gräfe, M. and Klauber, C. (2011) 'Bauxite residue issues: IV. Old obstacles and new pathways for in situ residue bioremediation', *Hydrometallurgy*. Elsevier B.V., 108(1–2), pp. 46–59.

Gräfe, M., Power, G. and Klauber, C. (2011) 'Bauxite residue issues: III. Alkalinity and associated chemistry', *Hydrometallurgy*. Elsevier B.V., 108(1–2), pp. 60–79.

Grzymek et al. (1979) 'Method for Obtaing Aluminium Oxide'. United States Patent US 4149898.

Habashi, F. (2005) 'A short history of hydrometallurgy', *Hydrometallurgy*, 79(1–2), pp. 15–22.

Hignett, T. P. (1947) 'PILOT PLANTS: Production of Alumina from Clay by a Modified Pedersen Process', *Industrial & Engineering Chemistry*, 39(8), pp. 1052–1060.

J.A. Apps, J. M. N. (1990) 'Correlation of the Solubilities of Aluminum Hydroxides and Oxyhydroxides in Al~aline Solutions with the Thermodynamic Properties of AI(OH) 4-', *Chemical Modeling of Aqueous Sytems*.

Jiayu Ma, Zhibao Li, Q. X. (2012) 'A New Process for Al2O3 Production from Low-Grade Diasporic Bauxite Based on Reactive Silica Dissolution and Stabilization in NaOH-NaAl(OH)4 Media', *AIChE Journal*, 58(7), pp. 2180–2192.

Klauber, C., Gräfe, M. and Power, G. (2011) 'Bauxite residue issues: II. options for residue utilization', *Hydrometallurgy*. Elsevier B.V., 108(1–2), pp. 11–32.

Li, X. Bin *et al.* (2013) 'Relationship between Al(OH)3 solubility and particle size in synthetic Bayer liquors', *Transactions of Nonferrous Metals Society of China (English Edition)*. The Nonferrous Metals Society of China, 23(5), pp. 1472–1479.

Li, Y. *et al.* (2009) 'Precipitating sandy aluminium hydroxide from sodium aluminate solution by the neutralization of sodium bicarbonate', *Hydrometallurgy*. Elsevier B.V., 98(1–2), pp. 52–57.

Meyer, F. M. (2004) 'Availability of bauxite reserves', *Natural Resources Research*, 13(3), pp. 161–172.

Miller, J. and Irgens, A. (1974) 'Alumina production by the Pedersen Process - History and future', *Light Metals 1974*, pp. 977–982.

Murer Hollum, A., Addison James, W. and Alexander Semple, W. (1951) 'Process of Producing Alumina From Slags or Sinters Prepared From Lime and Alumina-Bearing Mate-Rials'. United States Patent US 2544231.

Nedkvitne, E. (2018) *Slag making, leaching and preparations for precipitation experiments relating to the Pedersen process*.

Nielsen, K. (1978) 'The Pedersen Process - An old process in a new light', *Erzmetall*, pp. 523–525.

Noworyta, A. (1981) 'On the removal of silica fom aluminate solutions: mechanism and kinetics of the process', *Hydrometallurgy*, 7, pp. 99–106.

Panias, D. and Paspaliaris, I. (2003) 'Boehmite process-A new approach in alumina production', *Erzmetall*, 56(2), pp. 75–81.

Panov, A., Vinogradov, S. and Engalychev, S. (2017) 'Evolutional Development of Alkaline Aluminosilicates Processing Technology'.

Pedersen, H. (1927) 'Process of Manufactoring Aluminum Hydroxide'. United States Patents US 1618105.

Power, G., Gräfe, M. and Klauber, C. (2011) 'Bauxite residue issues: I. Current management, disposal and storage practices', *Hydrometallurgy*. Elsevier B.V., 108(1–2), pp. 33–45.

Rossiter, D. S. *et al.* (1998) 'Investigation of the unseeded nucleation of gibbsite, Al(OH)3, from synthetic bayer liquors', *Journal of Crystal Growth*, 191(3), pp. 525–536.

Safarian, J. and Kolbeinsen, L. (2016) 'Smelting-Reduction Of Bauxite For Sustainable Alumina Production', *Sustainable Industrial Processing Summit and Exhibition*, 5.

Shayanfar, S. *et al.* (2018) 'Aluminum hydroxide crystallization from aluminate solution using

carbon dioxide gas : Effect of temperature and time', *Journal of Crystal Growth*. Elsevier B.V., 496–497, pp. 1–9.

Smith, P. (2009) 'The processing of high silica bauxites - Review of existing and potential processes', *Hydrometallurgy*. Elsevier B.V., 98(1–2), pp. 162–176.

Tong, Z. and Li, Y. (2008) 'Leaching Behavior of ALumina from Smelting Reduction Calcium Aluminate Slag with Sodium Carbonate Solution', *Light Metals 2017*, The Minera, pp. 37–43.

Wang, Z. *et al.* (2005) 'Evolution of particle size and strength of hydrargillite from carbonization in seeded sodium aluminate liquors', *Journal of Crystal Growth*, 274(1–2), pp. 218–225.

De Weerdt, K. (2007) *SINTEF Report: Advanced cementing materials*. SINTEF Building and Infratructure.

Yao, Z. T. *et al.* (2014) 'A review of the alumina recovery from coal fly ash, with a focus in China', *Fuel*. Elsevier Ltd, 120, pp. 74–85. .

Zhang, D. *et al.* (2018) 'Alumina, iron and titanium extracting from bauxite residue with low lime sinter method', *Minerals, Metals and Materials Series*, Part F4, pp. 143–148.

Zhang, T. *et al.* (2016) 'Calcification - carbonation method for alumina production by using low-grade bauxite', *Minerals, Metals and Materials Series*, (210869), pp. 233–238.

Zhou, Q. *et al.* (2009) 'Hydrometallurgy Agglomeration of gibbsite particles from carbonation process of sodium aluminate solution', *Hydrometallurgy*. Elsevier B.V., 99(3–4), pp. 163–169.